12.0 INTERPRETATION OF CASE HISTORIES

12.1 INTRODUCTION

In this section, eight case histories are described: six have been previously published. Two case histories, LOOP Cavern #11 and the Kansas caverns #6 and #25, were kindly made available for this research project. The authors are indebted to Jay Russel (T&C Consulting), Rod Thiel (Ambitech Engineering Corporation), and Harold Osborne and Tom McCauley (LOOP Inc.) who provided data and helpful additional comments. Each of the eight case histories is described in a different section and the purpose of including the case histories are briefly described below.

Cases 1 Through 4 Included in Sections 12.2 to 12.5

The Etrez-1 case (Section 12.2) and the Carresse case (Section 12.3) are two examples of pressure increase or pressure drop tests during which pressure history and/or expelled liquid flow rate were carefully measured, which provides data for a precise assessment of the various factors (transient creep, brine warming, adiabatic pressure change, additional dissolution) contributing to the pressure histories.

Remizov et al. (Section 12.4) described an MIT where the transient phase was much shorter than what is observed during most other tests, which strongly suggests that each site has somewhat specific characteristics.

The EZ58 test (Section 12.5) comprises a tightness test performed on a well (rather than on a full-size cavern). With the "cavern" radius being extremely small, the relative significance of the various factors contributing to pressure evolution is drastically changed: brine permeation through the rock-mass, a negligible phenomenon in a cavern, plays a prominent role in the case of a well.

Cases 5 Through 8 Included in Sections 12.6 to 12.9

Case histories discussed in Sections 12.6 through 12.9 relate to the PDO (Pressure Difference Observation) Method.

The LOOP case (Section 12.6) and the Etrez-2 case (Section 12.7) prove that a leak at the wellhead (even through an extremely small leakage) can easily be detected by the PDO Method. The Etrez-3 case (Section 12.8) shows that the PDO Method is extremely accurate when the cavern neck is relatively narrow. The Kansas case (Section 12.9) shows that interpretation is more difficult when the shape of the cavern neck is irregular or absent; however, additional information (when compared to the standard Pressure Observation Testing Method) is provided by the PDO Method.

12.2 THE ETREZ TRANSIENT CREEP TEST (AFTER HUGOUT [1984])

12.2.1 Introduction

The EZ53 cavern is a 7,500 ± 500-m^3 cavern leached out at a depth of 950 m. The cavern shape is shown in Figure 31. Leaching of EZ53 was completed by June 6, 1982.

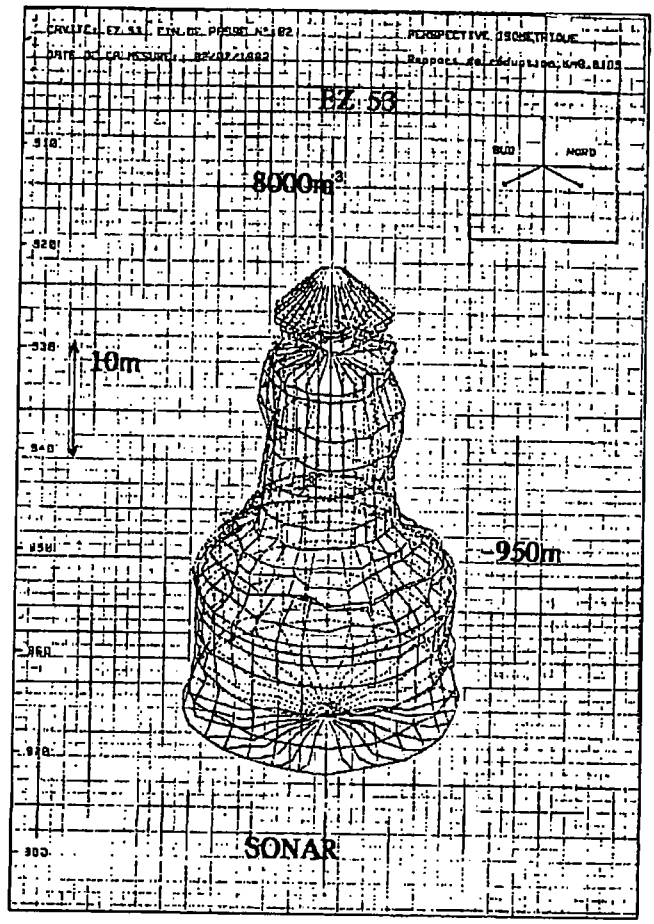

Figure 31. EZ53 Sonar Survey.

During the fall of 1982, a "transient creep" test was performed on the EZ53 cavern [Hugout, 1984]. The cavern had been kept idle for 3 months after cavern leaching was completed. The cavern pressure was then lowered by 3.4 MPa, kept constant for 160 days, and then increased back to halmostatic pressure, providing interesting data on the effects of rapid pressure

changes.[5] In the context of MIT interpretation, we are interested mainly in the pressure increase that took place less than 1 year after the cavern was leached out.

12.2.2 Cavern Behavior Before the Test

In the months following the end of leaching, brine warming resulted in brine thermal expansion, as described in Section 6.3. The cavern brine temperature was 35.22°C on September 8, 1982 (Day 94, or the day after the transient creep test began); 36.09°C on October 7, 1982 (Day 123); and 37.55°C on December 8, 1982 (Day 185). Assuming $V = 7{,}500$ m^3 and $\alpha_b = 4.4 \cdot 10^{-4}$/°C leads to an average volume increase rate of 100 liters per day during Days 94–123 and 80 liters per day during Days 123 to 185–an expansion rate decrease consistent with that discussed in Section 6.3.

The effect of cavern creep was assessed with a transient creep test. At a depth of 950 m, geostatic pressure is 21 MPa, and brine pressure in an open cavern (halmostatic pressure) is 11.4 MPa. An outflow of 180 liters per day was observed shortly before the creep test began. Steady-state creep was measured 8 years later [Brouard, 1998] and found to be 7 liters per day; however, creep is likely to have been faster just a few months after leaching was completed. The initial outflow rate is larger than can be explained solely by the effects of thermal expansion; cavern creep was probably faster during this period soon after leaching than it was 8 years later, after the cavern idled for a long period. Nonetheless, the information from the case history will be interpreted to isolate the expected thermal expansion effects.

12.2.3 Effects of Cavern Pressure Drop

The cavern pressure was decreased to assess the effect of lower cavern pressure on cavern creep rate. The annular space was filled with a light hydrocarbon, whose pressure at the wellhead was approximately $p_l^1 = 3.4$ MPa. On September 7, 1982 (Day 93), a valve was opened at the wellhead to partially remove the hydrocarbon; the hydrocarbon pressure at the wellhead decreased to atmospheric pressure; the air/brine interface in the central string dropped by $h_{int}^o = p_l^1/\rho_b g = 3.4 \cdot 10^6$ Pa/1,200 kg/m^3 /10 m/s^2 = 290 m to balance the pressure drop in the annular space. The hydrocarbon outflow rate was measured from Day 93 to Day 254 (Figure 32.a).

The hydrocarbon outflow rate during this period was governed by three main phenomena:

- *brine warming*: this effect accounts for 100 liters per day or more at the beginning of the test; however, the expelled fluid rate because of brine warming gently decreases with respect to time (adiabatic pressure drop followed by brine warming may also play a secondary role).

[5] The cavern pressure histories for the EZ53 are shown in the insert in Figure 33.

- *transient creep*: the cavern pressure drop (by 3.4 MPa) triggers transient creep. After some time, steady-state creep is again achieved, but is faster than the creep rate when the cavern pressure was at halmostatic pressure (because the difference between geostatic pressure and cavern pressure is increased from 21 – 11.4 = 9.6 MPa to 21 – 8 = 13 MPa).
- *brine crystallization:* This effect is triggered by a pressure drop. The total volume change induced by crystallization can be computed using the formulas given in Section 8.2.

RSI-1476-05-036

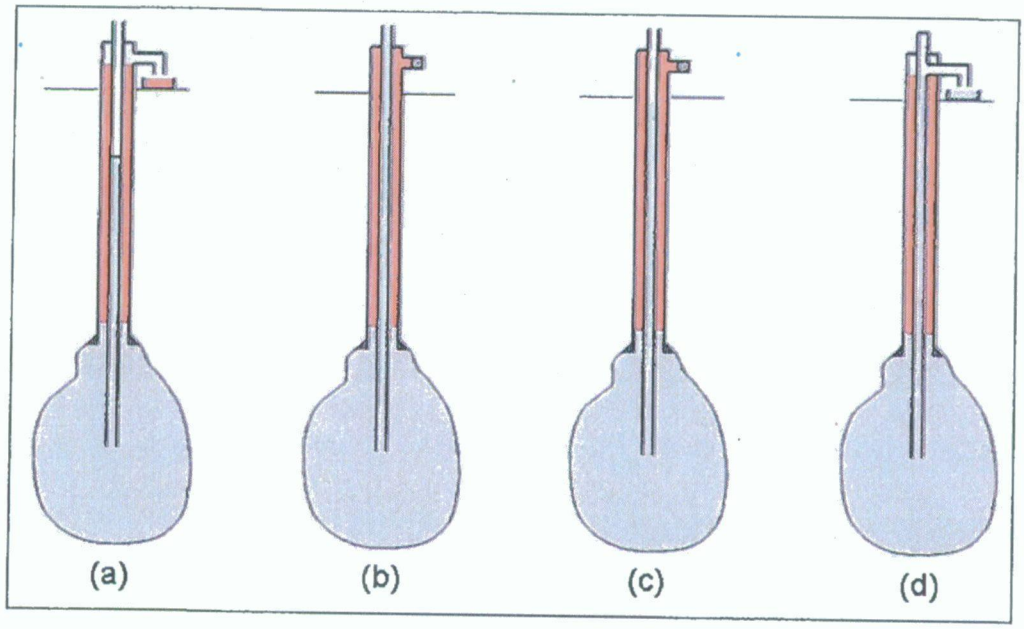

Figure 32. Evolution of Brine and Hydrocarbon in the Well at the End of EZ53 Transient Creep Test.

The amount of brine to be withdrawn during a rapid depressurization by $-p_t^1 = -3.4$ MPa is

$$v_o^{with} = S_t h_{\text{int}}^o - \left(\beta_E + \beta_b^{ad}\right) V p_t^1 = -\left(\frac{S_t}{\rho_b g} + \left(\beta_E + \beta_b^{ad}\right) V\right) p_t^1 \qquad (126)$$

Taking into account $\beta V = 3$ m³/MPa, $S_t = 21.1$ liters/m, $g = 10$ m/s², and $\rho_b = 1{,}200$ kg/m³, we have $v_o^{with} = -16.15$ m³. However, brine crystallization reduced the brine outflow because the brine volume is smaller than the sum of the volumes of its two components (salt and soft water). This effect was discussed in Chapter 8.0. However, because cavity pressure is kept constant, Equation (86) is replaced by:

$$V_c^f = V_b^f + S_t h_{\text{int}}^o \qquad V_c^o = V_b^o \qquad (127)$$

or

$$v^{with} = S_t h^o_{int} - \left(a_s - \varpi + \beta_E\right) V^o_c p^1_t \tag{128}$$

And the additional brine volume expelled from the cavern after depressurization is

$$v^{with} - v^{with}_o = -\left(a_s - \varpi - \beta^{sd}_b\right) V^o_c p^1_t \tag{129}$$

or with $a_s - \varpi - \beta^{sd}_b = 0.174 \cdot 10^{-4}$ /m^3-MPa and $V^0_c = 7{,}500 m^3$, $v^{with} - v^{with}_o = 444$ liters (2.8 bbls).

The combined effects of salt crystallization and cavern creep—two transient phenomena—are observed clearly in Figure 33. The expelled flow rate, which was 182 liters per day before the test, soars to 4,500 liters (28 bbls) per day immediately after the cavern pressure reduction and then rapidly decreases to: 280 liters per day by Day 113, to 200 liters per day by Day 143, and to 140 liters per day on Day 193.

12.2.4 Effects of Cavern Pressure Increases

The cavern halmostatic pressure was restored on Day 253. This phase of the test is of special interest for this research because it simulates an MIT. The annular space was closed at the wellhead and the central tubing was filled with brine (Figure 32b). After this injection was completed, the brine level dropped in the central tubing (an effect of additional dissolution and transient cavern creep (Figure 32c)). Every 24 hours, brine was added to fill the central tubing. The daily amount of brine added gradually decreased. Eventually, 10 days after the first filling took place (Day 263), brine was again expelled from the wellhead (see Figure 33), and a constant brine-flow rate was observed equivalent to 52 liters per day. The difference between the brine expulsion of 182 liters per day at the start (soon after leaching) and the 52 liters per day at the end is because brine thermal expansion is less active 1 year after cavern leaching was completed.

During Days 254–265, brine dissolution and transient creep (cavern volume *increases* during this period) are active. A tentative analysis can be performed.

During this period of time, the total amount of brine injected (–) or withdrawn (+) was carefully measured:

$$-393 - 220 - 171 - 138 - 32 - 32 - 33 - 33 - 34 - 68 + 31 + 48 = -1{,}077 \text{ liters (6.8 bbls)}.$$

During the same 12-day period, the effects of brine thermal expansion and steady-state creep were the same as they would be couple of weeks later; i.e., 52 liters per day (0.33 bbls/day), or 624 liters (3.9 bbls) during the 12-day period. The effect of adiabatic pressure increase followed by brine cooling is approximately 50 liters and is not taken into account.

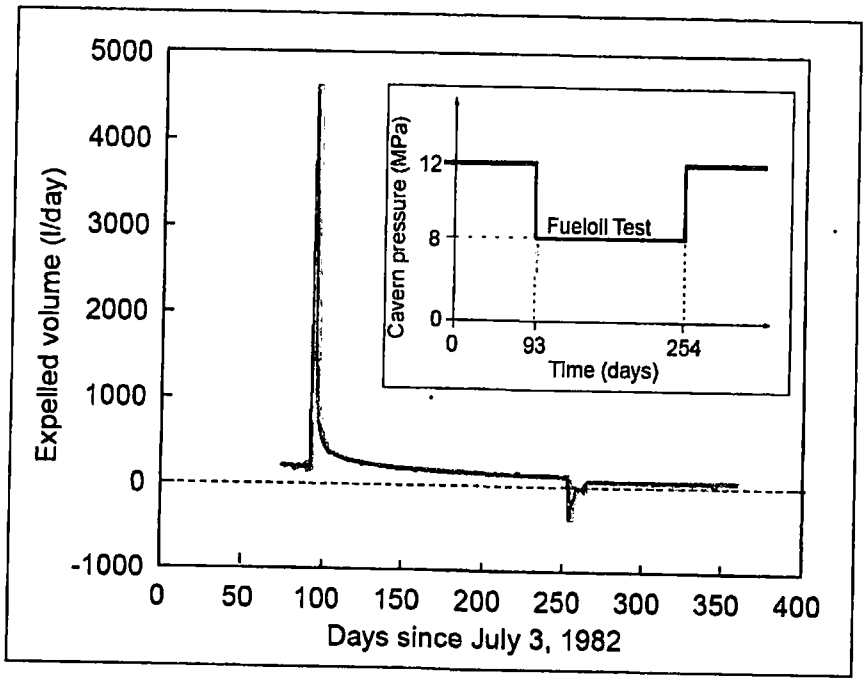

Figure 33. EZ53 Transient Creep Test (After Hugout [1984]). The initial cavern pressure at a depth of 950 m is 11.4 MPa rather than the 12 MPa shown, making the actual cavern pressure reduction equal to 3.4 MPa.

The cumulative effects of additional dissolution and transient creep during this 12-day period is 1077 + 624 = 1,700 liters (10.7 bbls).

The effect of additional dissolution can be computed easily using the formula given in Section 12.2.3:

$$v^{inj} - v_o^{inj} = \left(a_s - \varpi - \beta_b^{ad}\right) V_c^o p_i^1 = 444 \text{ liters (2.8 bbls)} \qquad (130)$$

In other words, transient creep is responsible for a cavern volume increase of 1,700 – 444 = 1,256 liters (7.9 bbls). In this example, the effect of additional dissolution is 1/3 of the effect of inverse transient creep.

12.3 CARRESSE SPR3 TEST

A test was performed in the SPR3 cavern, an 11,000-m^3 brine-filled cavern leached out from a bedded-salt formation in southwestern France. The cavern depth is 692 m to 705 m. The cavern idealized-shape mesh used for computations is shown in Figure 34. The cavern had been kept idle (brine pressure at cavern depth was 8.25 MPa) for a very long period of time before the test was performed: brine warming was negligible in this context.

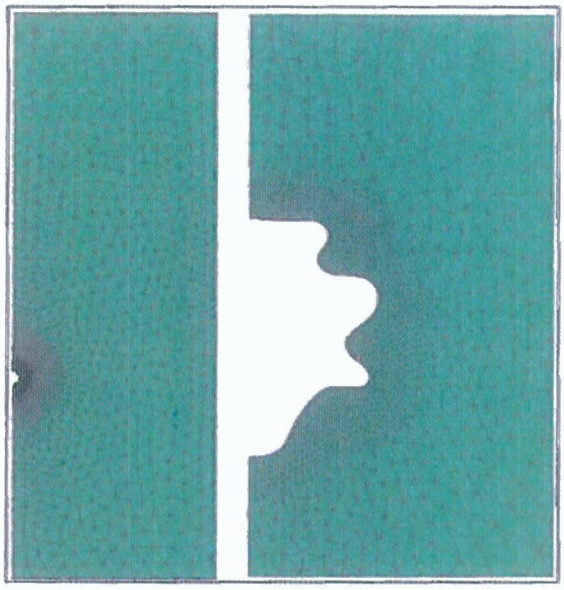

Figure 34. SPR3 Cavern Mesh Used for Numerical Computations.

This test consisted of increasing or decreasing cavern pressure through rapid liquid injection or rapid withdrawal. Five different steps occur, with each step lasting approximately 1 month (Figure 35). During the first step, the pressure consistently decreases (from 11.25 MPa to 10.75 MPa); conversely, during Steps 2, 3, and 4, pressure increases in the cavern. This can be explained by the combined effects of steady-state creep and steady-state brine permeation. (The effects of these two mechanisms are exactly equal when cavern pressure is approximately 10 MPa; when cavern pressure is larger than this value, the volumetric brine permeation rate is greater than the volumetric cavern creep rate, resulting in a pressure drop; the inverse is true when cavern pressure is less than 10 MPa.)

We are primarily interested in the transient pressure evolution that can be observed after pressure changes. Two mechanisms were taken into account (in addition to brine permeation):

1. Additional dissolution (the characteristic time (as defined in Chapter 8.0) was $t_c^{diss} =$ 2.5 days)
2. Transient creep.

The following parameters of the Munson constitutive law (see Section 9.4) were considered:

$$A \cdot \exp\left(-\frac{Q}{\Re T_R^{\infty}}\right) = 0.9 \cdot 10^{-8} \text{ /day-MPa}^{3.1} \quad \text{and} \quad n = 3.1$$

$$\delta = 0.58, \quad K_o = 1.9 \cdot 10^{-3} \text{ /MPa}^{3.1}, \quad \alpha_w = 6, \quad \beta_w = 0, \quad m = 1.3$$

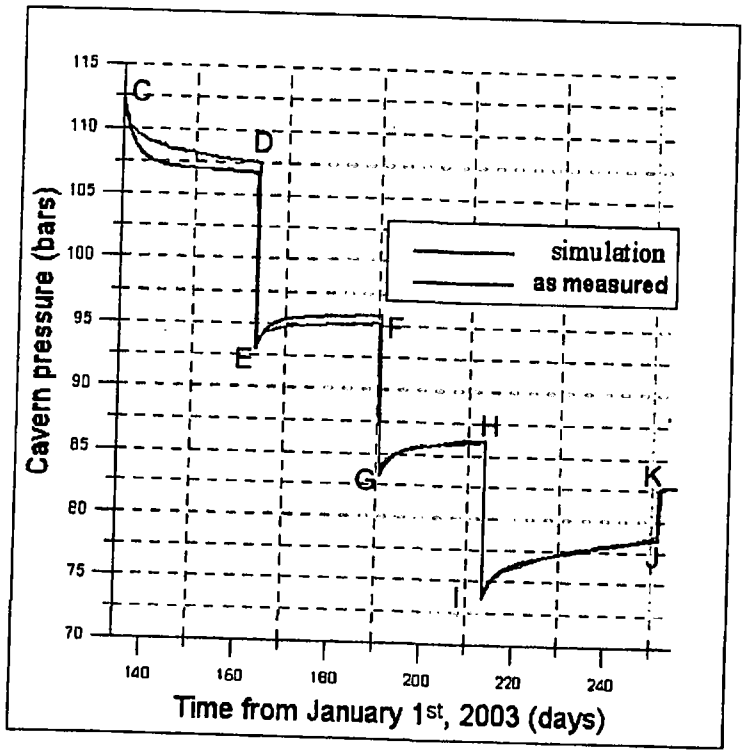

Figure 35. Comparison of as-Measured and as-Calculated Cavern Pressure Evolution.

The steady-state parameters (A, $\exp(-Q/\Re T_R^{-})$, and n) were back-calculated against field data to match the 22.5 liters/day expelled when the cavern was open. The parameter δ was chosen according to Munson [1997].

The agreement between the as-measured and the computed pressure evolution is good, as shown in Figure 35.

12.4 TRANSIENT EFFECT DURING MIT (AFTER REMIZOV ET AL. [2000])

Remizov et al. [2000] discussed the transient effects in a salt cavern during a tightness test: *"Due to plastic deformation of rock salt the test pressure drops even in a tight cavern...one should start reading the wellhead pressure drop after keeping the reservoir at the test pressure for 1-2 days."* Remizov result is remarkable in that transient effects duration is much shorter than what was observed during most tests described in the literature. Two examples are provided (Figure 36), but no detailed information is given.

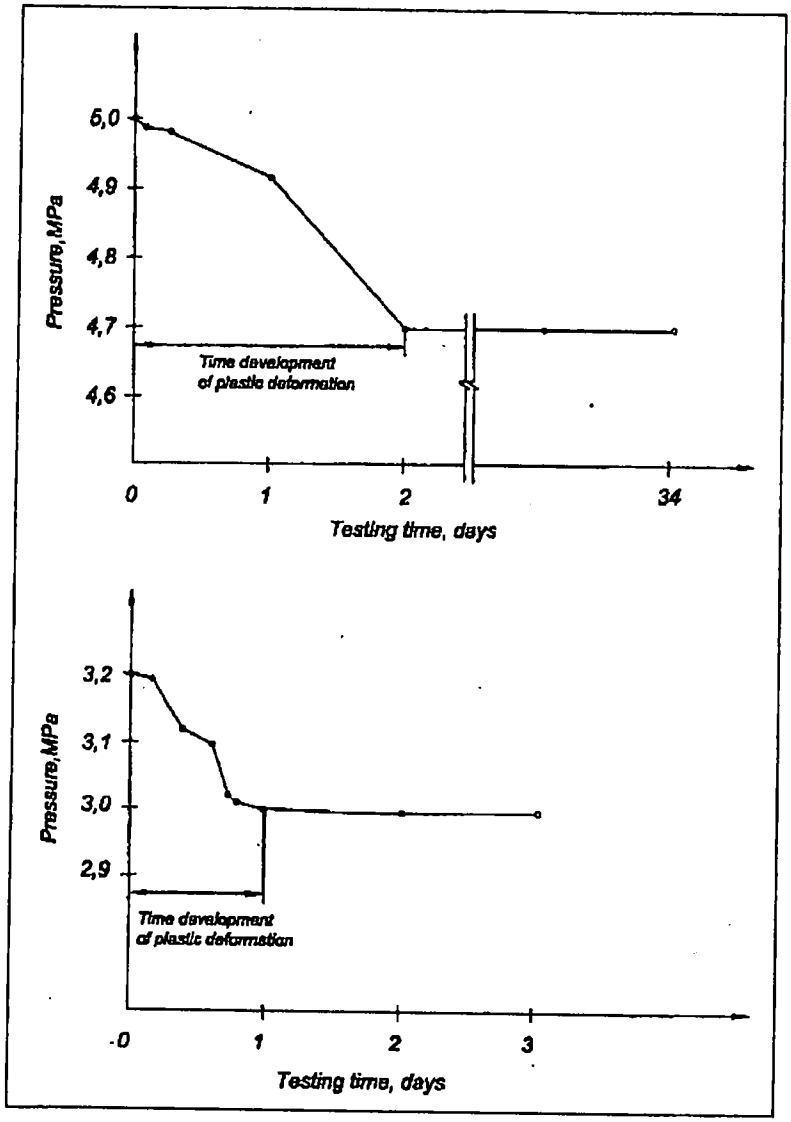

Figure 36. Cavern Pressure Evolution (After Remizov et al. [2000]).

12.5 ETREZ EZ58 TEST [DURUP, 1994]

EZ58 is a wellbore, not a cavern. This example is included for the pronounced permeation effect shown. The well is cased and cemented down to a 970.8-m depth; the depth of the well bottom is 1,169 m. No cavern was created, and the well diameter is 8½ inches (21.6 cm). During a 1-year-long test (supported by SMRI to assess salt micropermeability), the brine pressure was increased incrementally from halmostatic pressure to geostatic pressure. Brine was injected into the well daily to keep the well pressure constant between pressure increases. In such a small "cavern" (as a 21.6-cm large well certainly is), the respective roles of the various

mechanisms discussed in Chapters 5.0 to 9.0 are not the same as in a "standard" cavern. Because the well radius is small, brine warming is a fast phenomenon and thermal equilibrium is rapidly reached, and brine thermal expansion plays no role except immediately after a pressure change. Transient creep and additional dissolution are effective; however, transient and steady-state permeations play a dominant role. The characteristic hydraulic time, t_c^{hyd}, is inversely proportional to the square of the cavern radius: it is a few days in a well with a diameter of 20 cm. The transient evolution of the injected brine-versus-time curve, clearly observed in Figure 37, is governed by transient brine permeation–a negligible mechanism in a "standard" cavern.

RSI-1476-05-041

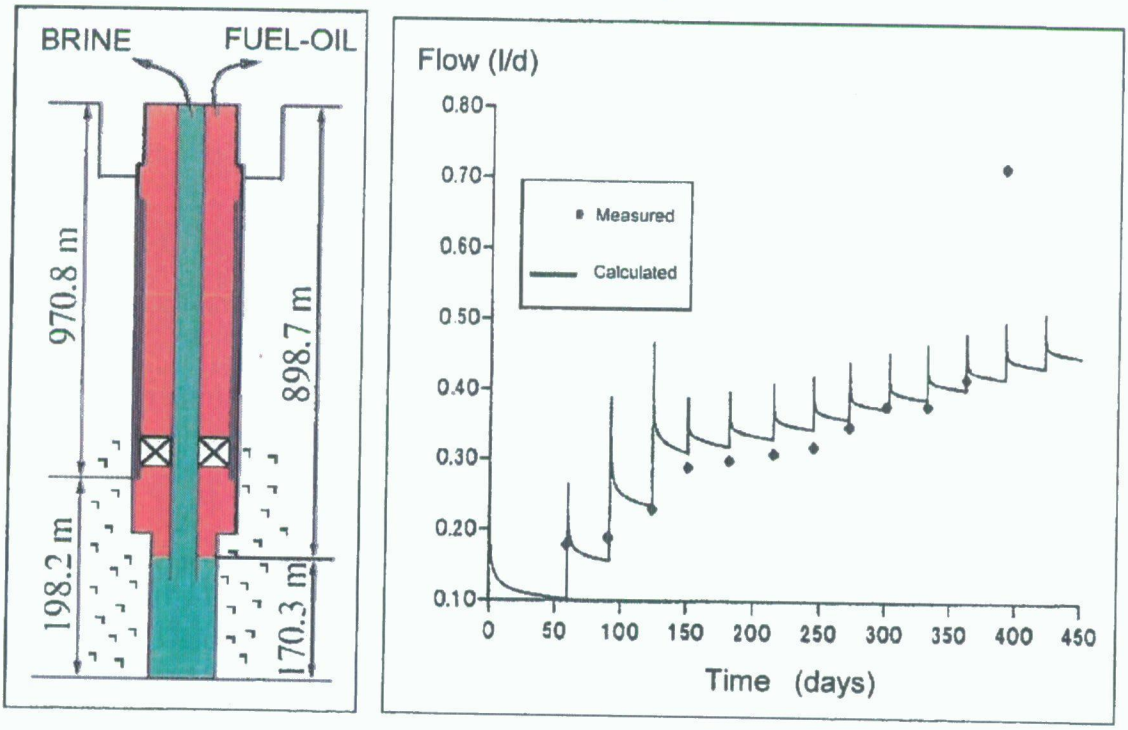

Figure 37. EZ58 Test (After Durup [1994]). Pressure drop is caused by transient brine permeation, an effect that is negligible in a full-size cavern but can be observed in a small-diameter well.

12.6 LOOP CAVERN MECHANICAL INTEGRITY TEST ANALYSIS

LOOP Inc. operates and maintains nine underground crude oil storage caverns in the Clovelly salt dome located in Galliano, Louisiana. Cavern #11 was pressure-tested between August 11 and August 17, 2002. Cavern #11 is a 7.526-million-barrel cavern with a casing seat depth of 1,616 feet below mean sea level (bmsl) and a cavern floor depth of 2,692 feet bmsl.

On July 11, 2002, the "final" oil transfer out of the cavern was made. On August 10, over a 6-hour period from 16:00 to 22:00, a 100,593-barrel exchange of oil (density 0.8185) for brine (density 1.196) was made. On August 11, the cavern pressure was increased from 337 psi to 603 psi over approximately a 5.5-hour period.

By the evening of August 16, the cavern pressure had stabilized sufficiently (572.5 psi compared to the starting pressure of 603 psi) to begin the official 24-hour pressure-monitoring test. The 1.3-psi pressure loss over the next 24-hour period (by 18:00 on August 17) compared favorably to a maximum allowable pressure loss of 2.0 psi/day. During the stabilization and test periods, both the product and brine wellhead pressures were recorded using calibrated equipment (Figure 38).

RSI-1476-05-042

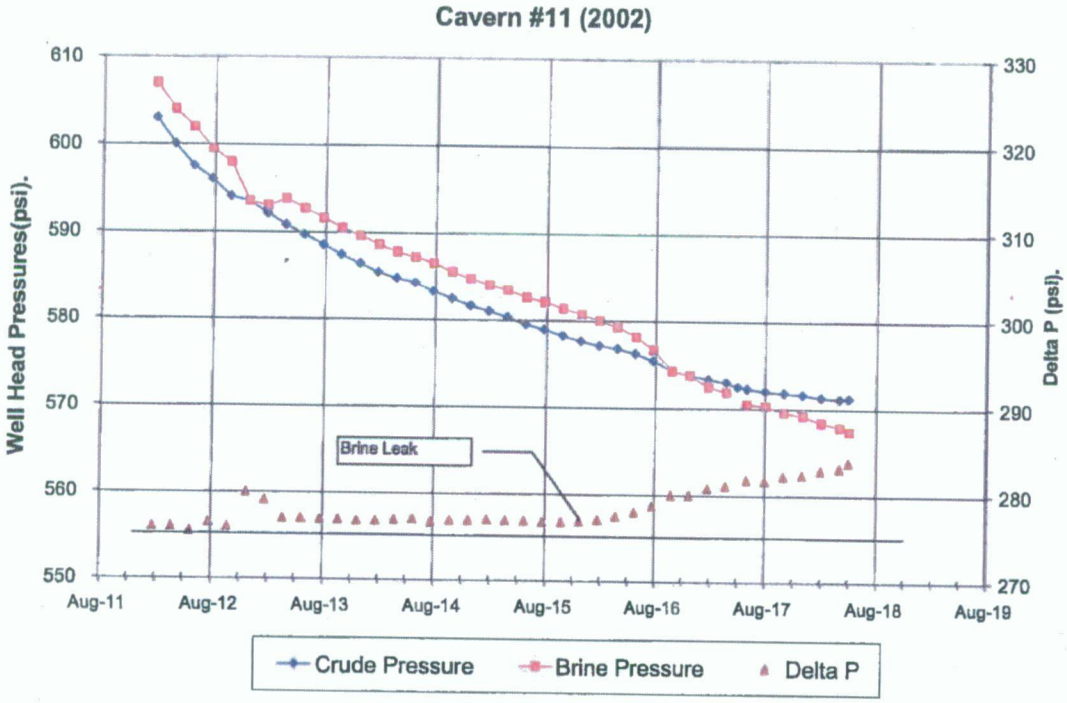

Figure 38. LOOP Cavern 11 MIT From 2002 (ΔP Is the Crude Oil Pressure Minus the Brine Pressure Both Measured at the Wellhead).

The following tentative interpretation can be made:

1. About a 30-day stabilization period elapsed between the final brine injection (oil withdrawal) and the MIT. Enough time was probably allowed to ensure full saturation of the brine injected into the cavern. The injected brine was colder than the rock-mass at cavern depth. In this very large cavern, brine warming is very slow (the cavern is a cylinder, height 300 m, radius $R = 35$ m; the characteristic time is $R^2/\pi k^{th}_{salt} = 4$ years).

It is difficult to be more specific because the initial brine, oil, and rock temperatures are not known. The pressure increase rate caused by brine warming is probably slower than 1 psi/day (in a cylindrical cavern, the brine temperature evolution following a cavern brine temperature change by ϑ_l^1 can be described by the following relation $\dot{\vartheta}_l / \vartheta_l^1 = (0.26/R)\left(1/\sqrt{t}\right)$, R in meters, t in days, and $\dot{p}_l = \alpha_b \dot{\vartheta}_l / \beta$, see Section 6.3.9).

2. The day before the pressure was increased, an oil injection was made to push the oil level down, and on the day of the pressure increase, oil was again injected. The temperature of this oil was not measured. If the oil was cooler, it would have been warmed with time and its volume would have increased, resulting in an increase in brine pressure and a decrease in oil column density when the cavern was shut in. These effects would lead to an underestimation of an actual leak during an MIT because pressure drop caused by liquid loss will be masked by the pressure increase caused by oil warming. However, oil-warming in the well would have been a fast process because the well radius is small (see Section 6.1).

3. Before the test begins, the pressure difference, or "Delta P", is 276 psi, or 1.94 MPa

$$P_{ann}^{wh} - P_{tub}^{wh} = -(\rho_b - \rho_o) g h \qquad (131)$$

where ρ_b is the saturated brine S.G. (1,196 kg/m^3), ρ_o is the oil S.G. (818.5 kg/m^3), and g is the gravitational acceleration (9.8 m/s^2); we have $\rho_b - \rho_o$ = 377.5 kg/m^3. The oil/brine interface is $h = \left(P_{ann}^{wh} - P_{tub}^{wh}\right) / \left[g(\rho_b - \rho_o)\right]$ = 520 meters (1,700 ft); i.e., deeper than the casing depth which is 1,616 feet, or 493 meters. The cavern volume is $V = 7.526 \cdot 10^6$ bbls, or $1.25 \cdot 10^6$ m^3. The compressibility factor is not known; $\beta = 4 \cdot 10^{-4}$/MPa or $3 \cdot 10^{-6}$/psi leads to βV = 500 m^3/MPa.

4. The blue curve (crude oil pressure versus time) probably reflects, more or less, the actual cavern pressure evolution, because no or small changes of the oil column density or height take place during the test (see below). From Day August 11 at 11:30 to August 12 at 11:30, the pressure evolutions are nonlinear. Transient effects are mostly effective during this period and include additional dissolution, adiabatic pressure change, and transient creep. They are probably still active for several more days. The changes in the red curve (brine pressure versus time) are probably because of brine leaks at the wellhead.

5. From August 12 at 11:30 to Day August 15 at 07:30, the pressure slope is almost constant and no pressure difference evolution is observed. The pressure drop rate during this period is slightly faster than $\dot{P}_{ann}^{wh} \approx \dot{P}_{tub}^{wh}$ = 4 psi/day. Remember that this figure is the "apparent leak." Thermal expansion effects should be added (however, they are likely to be smaller than 1 psi/day). Taking into account the cavern compressibility value (500 m^3/MPa, or 21 bbls/psi), as shown below, the apparent leak is large:

$$Q_{app} = \beta V \cdot \dot{P}_{ann}^{wh} = 4 \text{ psi/day} \times 21 \text{ bbls/psi} = 84 \text{ bbls/day } (14 \text{ m}^3\text{/day}) \qquad (132)$$

6. The apparent leak value may include (1) an oil leak, (2) a brine leak through the casing or through the wellhead, (3) a brine leak through the cavern wall, and (4) the effects of additional dissolution and transient creep. Items (1) and (2) are not likely to play a role during this phase, because no pressure-difference change is observed during this phase.

7. To describe the conditions associated with an oil leak, the following quantities are defined:

   - Let Q_{leak} be the actual oil leak (m^3/day or bbls/day).
   - Let Q be the brine or cavern volume change caused by such phenomena such as transient creep, additional dissolution, etc.
   - Let βV be the cavern compressibility (m^3/MPa or bbls/psi).

   The pressure drop rate at the brine string wellhead is

$$\frac{dP_{tub}^{wh}}{dt} = -\frac{(Q+Q_{leak})}{\beta V} \tag{133}$$

   The crude oil pressure in the annular space (P_{ann}^{wh}) decreases by an even larger amount than the pressure drop in the brine string. Let Σ be the cavern neck cross-sectional area at the oil/brine interface depth (m^2). The interface rise rate is q_o/Σ. Because the interface rise, the annulus column weight is heavier by $(\rho_b - \rho_o) g Q_{leak}/\Sigma$, resulting in an additional pressure drop rate:

$$\frac{dP_{ann}^{wh}}{dt} = -\frac{(Q+Q_{leak})}{\beta V} - \frac{(\rho_b - \rho_o) g Q_{leak}}{\Sigma} \tag{134}$$

   The pressure difference, or $P_{ann}^{wh} - P_{tub}^{wh}$, decreases by

$$\frac{dP_{ann}^{wh}}{dt} - \frac{dP_{tub}^{wh}}{dt} = -\frac{(\rho_b - \rho_o) g Q_{leak}}{\Sigma} \tag{135}$$

   The as-observed pressure difference rate forms the basis for the assessment of the oil leak rate (Q_{leak}) when the cross-sectional area (Σ) is known.

   The oil leak in the LOOP 11 cavern is likely to be zero or small, provided that the cross-sectional area at oil/brine interface depth, or Σ, is small. Let Σ be 1 m^2; the pressure difference rate is

$$\frac{dP_{ann}^{wh}}{dt} - \frac{dP_{tub}^{wh}}{dt}\ (\text{kPa/day}) = 3.7 \times Q_{leak}\ (\text{m}^3/\text{day}) \tag{136}$$

A 1-m^3/day oil leak would induce a 0.5-psi/day (3.7 kPa/day) pressure-difference drop rate. The actual drop rate during Days August 13 and 14 is clearly much smaller than 0.5 psi/day. It is interesting to note that the additional brine-pressure drop rate because of the oil leak alone would be

$$\delta\left(\frac{dP_{tub}^{wh}}{dt}\right)=-\frac{Q_{leak}}{\beta V} \tag{137}$$

A 1-m^3/day leak rate would result in a 3-kPa/day (0.44 psi/day) (additional) brine-pressure drop rate and a 5.7-kPa/day (additional) oil-pressure drop rate.

8. Consider the case of only a brine leak through the wellhead represented by Q_b^{wh}, and no leak though the casing or casing shoe ($Q_{leak}=0$). Then, the oil pressure drop rate is

$$\frac{dP_{ann}^{wh}}{dt}=-\frac{\left(Q_{leak}+Q_b^{wh}\right)}{\beta V} \tag{138}$$

The brine pressure at the wellhead, P_{tub}^{wh}, decreases by a larger amount than the annulus (oil) pressure drop. Let S_t be the cross-sectional area (m^2) of the tubing string. We assume that brine in the tubing is unsaturated (cavern brine is saturated.) Let ρ_u be the unsaturated brine, S.G ($\rho_u < \rho_b$). There exists in the tubing string an interface between saturated and unsaturated brine. The interface rise rate is Q_b^{wh}/S_t. If the interface rises, the string column weight will become heavier by $(\rho_b-\rho_u)gQ_b^{wh}/S_t$; ρ_b is the saturated brine, S.G. (1,200 kg/m^3), ρ_u is unknown unsaturated brine density; g is the gravity acceleration (9.8 m/s^2); S_t is the approximately 0.25 m^2, or 4.5 bbls/ft for a string diameter of 22 inches. The brine-pressure drop rate is

$$\frac{dP_{tub}^{wh}}{dt}=-\frac{\left(Q_{leak}+Q_b^{wh}\right)}{\beta V}-\frac{(\rho_b-\rho_u)gQ_b^{wh}}{S_t} \tag{139}$$

The pressure difference, or $\dot{P}_{ann}^{wh}-\dot{P}_{tub}^{wh}$, increases by

$$\frac{dP_{ann}^{wh}}{dt}-\frac{dP_{tub}^{wh}}{dt}=\frac{(\rho_b-\rho_u)gQ_b^{wh}}{S_t} \tag{140}$$

Note that the pressure difference *decreases* in the case of an oil leak from the annulus and *increases* in the case of an unsaturated brine leak from the tubing.

9. During August 16 and 17, the pressure difference increases by approximately 3.5 psi/day, or 25 kPa/day. Hence,

$$(\rho_b-\rho_u)Q_b^{wh}=S_t\left(dP_{ann}^{wh}/dt-dP_{tub}^{wh}/dt\right)/g=600 \text{ kg/day} \tag{141}$$

For example, if $\rho_b - \rho_u$ = 100 kg/m^3, the brine leak is 6 m^3/day; if $\rho_b - \rho_u$ = 10 kg/m^3, the brine leak is 60 m^3/day.

We tried to assess the unsaturated and unknown brine (or string brine, ρ_u) density. Unfortunately, our results were inconsistent.

On August 12 at 7:30, the brine pressure decreased and $P_{ann}^{wh} - P_{tub}^{wh}$ increased. This event is probably related to a brine leak that stops after a few hours. (The leak may have been through a pinhole that plugged itself after some time by salt crystallization.) The brine-pressure drop rate from August 12, 3:30 to 7:30, is slightly faster than dP_{tub}^{wh}/dt = −1 psi per hour (or 7 kPa per hour).

Surprisingly, the oil-pressure drop rate seems to decelerate during this phase, although it should not. It is difficult to be sure that this deceleration is linked to the leak onset, because the slope of the oil pressure-versus-time curve is somewhat erratic during this phase.

The oil pressure evolution for August 12 is hypothetically explained as follows. The geothermal gradient in the well is, say, 3°C/100 meters. Assume that the leakage period is 6 hours and the leak rate is 22 bbls/hour. The interface rise rate is 5 meters/hour. The brine column rises by 6 hours × 5 meters/hour = 30 meters, and the temperature in the well (from top to bottom) increases by 1°C because of the warmer oil temperature. This temperature difference declines with time and equilibrium is reestablished after several hours; as this occurs, the brine in the well cools and becomes heavier, resulting in a pressure drop. The oil temperature warms by, say, 0.5°C and cools down later to reach thermal equilibrium. The oil thermal-expansion coefficient is, $\alpha_o = 10^{-3}$/°C. When the oil column warms by 1°C, its density decreases by 830 kg/m^3 × 10^{-3} /°C × 0.5°C = 0.4 kg/m^3. The column height is 500 m. The oil pressure increases by 0.4 kg/m^3 × 9.8 m/s^2 × 500 m = 2 kPa, or 0.3 psi. However, this pressure build-up is too small when compared to the as-observed slope change in the oil pressure-versus-time curve.

12.7 LEAK DETECTION (PDO) AT THE WELLHEAD

The absence of a wellhead leak can be determined as follows. A small amount of hydrocarbon (1 bbl) is injected into the central tubing. Any hydrocarbon leak through the wellhead will result in a rise of the hydrocarbon-brine interface in the central tubing and an increase in the pressure difference. The rate of the pressure difference increase is

$$\frac{dP_{ann}^{wh}}{dt} - \frac{dP_{tub}^{wh}}{dt} = (\rho_b - \rho_h) g \frac{Q_{tub}}{S_t} \tag{142}$$

where Q_{tub} is the hydrocarbon leak rate (through the tubing wellhead) and S_t is the central tubing cross section. Note that the pressure difference increases, as was observed during the

LOOP Cavern #11 test (described in the previous section), when a brine leak appeared at the wellhead. An example of this is provided in Figure 39.

RSI-1476-05-043

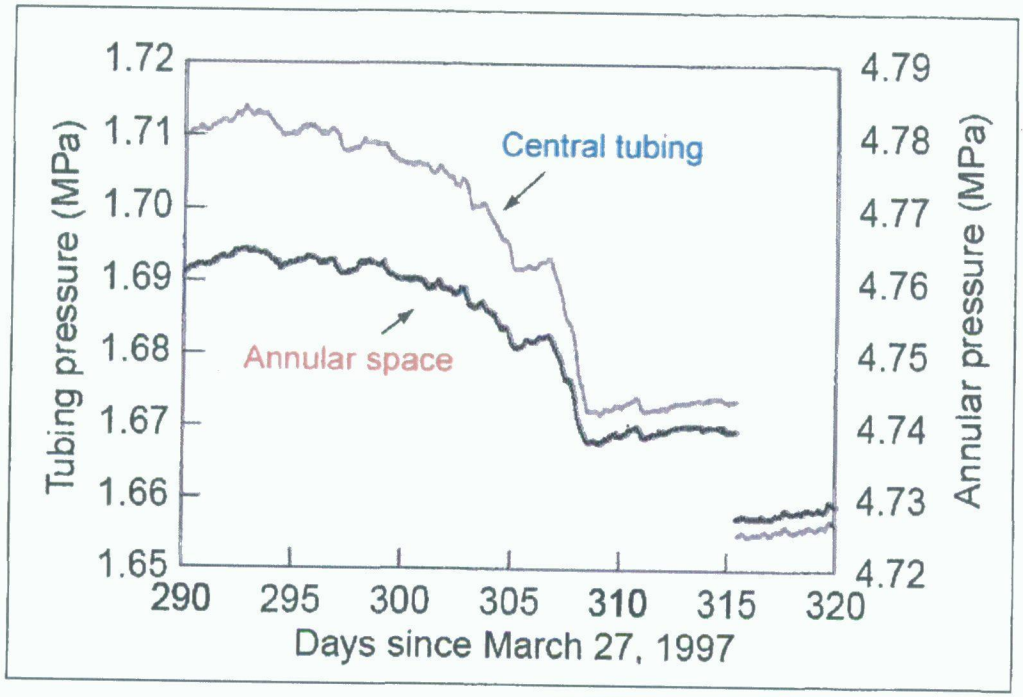

Figure 39. Annular Space and Tubing Pressure During a Well Leak. The two curves are parallel before Day 293 (no leak) and after Day 315 (leak repaired). During Days 293–315, the difference $P_{ann}^{wh} - P_{tub}^{wh}$ increases. Note that in the figure the P_{ann}^{wh}-versus-time curve is below the P_{tub}^{wh}-versus-time curve after Day 315.

A test was performed on the EZ53 cavern described in Section 12.2 and pressure history shown in Figure 39. Between Days 290 to 293, the pressure difference $\left(\Delta P = P_{ann}^{wh} - P_{tub}^{wh}\right)$ is fairly constant. (In fact, there was a small negative pressure difference rate of approximately 60 Pa/day; it is suspected that there was a tiny hydrocarbon leak from the annular space to the central tubing.) On Day 293, a rapid and severe increase of the pressure difference took place—clear evidence of a hydrocarbon leak through the central-tubing wellhead. The cumulative change in pressure difference from Day 293 to Day 314 is δP = 21 kPa, which proves that the hydrocarbon leak during this phase is $V_{leak} = S_t \delta P / g(\rho_b - \rho_h)$ = 124 liters. The average leak rate is Q_{tub} = 6 liters per day. (Fluid density in this specific case is ρ_h = 850 kg/m^3; the tubing cross section is S_t = 21.1 l/m.) On Day 315, the leak was repaired. (Note that the leak was detected through pressure data observation before being observed in the field.)

12.8 PDO TEST IN EZ53 CAVERN

A Pressure Difference Observation (PDO) test was performed on the EZ53 cavern, a brine-filled cavern at the Etrez site operated by Gaz de France. The main objective of this test (supported by the SMRI [Bérest et al., 2001b]) was not to test any MIT method, but it does allow us to assess the PDO method.

The EZ53 cavern depth is 950 meters and the cavern volume is 7,500 ± 500 m^3. The well completion includes a 9 5/8-inch cemented casing and a 7-inch string. The casing shoe depth is 846 meters. Cavern compressibility was measured as $\beta V = 3$ m^3/MPa (0.13 bbls/psi).

The well was tested in 1997–1998, 16 years after the cavern was leached. In a small and idle cavern, after such a long period of time, brine thermal expansion can be disregarded (the thermal characteristic time, as defined in Section 6.3.3, is 6 months–much shorter than 16 years). On March 20, 1997, a liquid hydrocarbon column (density = ρ_h = 850 kg/m^3) was injected into the annular space, creating an interface depth of 864 meters (below the casing shoe), where the horizontal cross section of the annular space is Σ = 5.7 l/m. (The cavern neck is an almost perfect cylinder.) On March 27 (Day 1), the cavern pressure was increased by 3 MPa. During the following 4 months, small amount of fluids were injected into and withdrawn from the cavern, but no large pressure changes were experienced. In this context, the effects of transient creep and additional dissolution can be disregarded.

Figure 40 displays the change of the wellhead pressures as recorded during Days 112–142. Pressures were measured with Rosemount pressure gauges (Model 3051 CG) with a resolution of ± 0.5 kPa and a maximum drift of ± 0.3 kPa per year. The rate of average pressure decrease is $\dot{P}^{wh}_{ann}$ = –869.70 Pa/day in the annular space and $\dot{P}^{wh}_{tub}$ = –869.85 Pa/day in the central tubing. The two curves are almost perfectly parallel. The following interpretations were made:

- The apparent well leak is $\beta V \cdot \dot{P}^{wh}_{tub}$ = 2.6 liters/day (8 m^3/year or 50 bbls/year). This apparent leak cannot be attributed to transient creep or additional dissolution. In fact, the cavern was leached in a bedded salt formation, where the insoluble content is approximately 10 percent. It is suspected that this small leak originates from brine micropermeation into the salt and/or insoluble layers at the cavern wall.
- The hydrocarbon leak, or $Q_{leak} = \Sigma\left(\dot{P}^{wh}_{tub} - \dot{P}^{wh}_{tub}\right)/(\rho_b - \rho_h)g$, is exceedingly small (less than 1 liter per year).

Note that very small fluctuations (period = approximately 12h; amplitude = 0.5 kPa or 0.07 psi) can be observed on the two pressure-versus-time curves. These fluctuations can be attributed to ground-level temperature changes and earth tides.

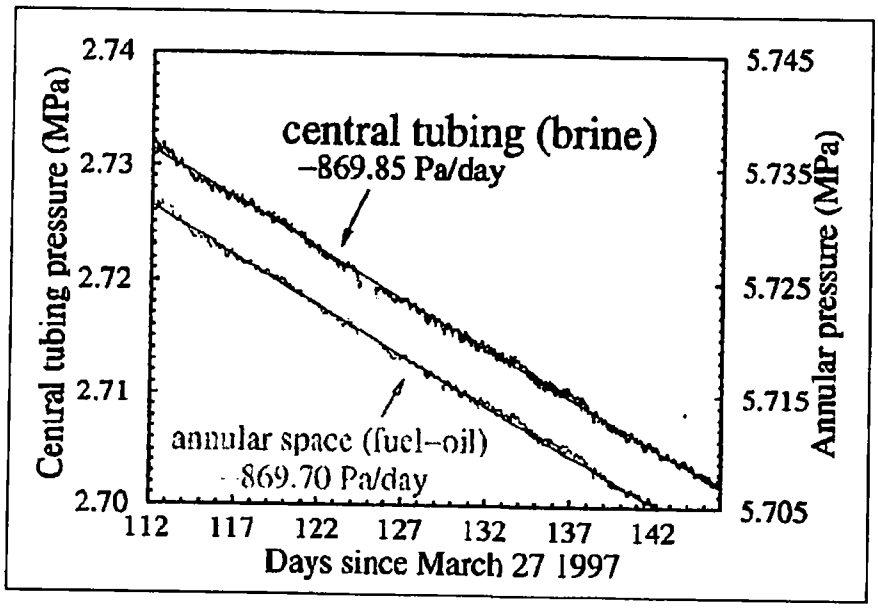

Figure 40. Annular Space and Central-Tubing Pressure Drops. The two curves are almost perfectly parallel, a clear sign that there is no well leakage.

Clearly, this test was exceptional: thermal expansion did not occur, and a very long stabilization period (4 months) occurred before the test—two conditions that can not be met during most real-life MITs. However, it was proven in this case that (a) the total leak was very small (50 bbls/year), and (b) the hydrocarbon leak through the casing or casing shoe was either zero or exceedingly small.

12.9 KANSAS MECHANICAL INTEGRITY TESTS

As described in the next section, Kansas salt caverns present a particular set of testing concerns for MITs compared to the factors influencing MITs in most other locations. Thiel and Russel [2004] have performed dozens of MIT tests in bedded salt caverns in Texas and Kansas. They kindly provided recent data obtained from two POTs (Pressure Observation Tests) in so-called Cavern #6 and Cavern #25 located in the shallow Hutchinson salt formation in Kansas. The analysis of the POT data will be presented followed by a discussion of how the same test data can be (or why it can not be) reinterpreted as an example of Pressure Difference Observation test.

The current test objective for Kansas MITs is to prove cavern integrity to within 1,000 bbls per year. A 1,000-bbls/year minimum resolution for a cavern test has become a de facto standard; however, the Kansas Department of Health and Environment (KDHE) in Kansas is still working to establish its regulatory standard for minimum acceptable test resolution.

12.9.1 Introduction

The two MITs selected as case histories are described in detail by Thiel and Russel [2004]. A brief synopsis is repeated here to aid in understanding the later discussion.

The two cavern MITs were conducted in Wells #6 and #25, LPG-storage caverns in Kansas. The architectures for Well #6 and Well #25 are presented in Figures 41 and 42, respectively. These caverns are relatively shallow: the floor of Well #6 is at 636 feet and the roof is at 587 feet. For Well #25, the floor is at 594 feet and the roof is at 450 feet. The volumes of the caverns are 242,000 and 127,000 bbls, respectively.

The cavern compressibility was measured at the outset of the testing and the measurement data are shown in Figures 43 and 44 for Well #6 and Well #25, respectively. As shown in the figures, which are reproduced from Thiel and Russel [2004], the total injection volume and rate of brine injection were 48.8 bbls at 0.51 bbl/min for Well #6 and 38.1 bbl at 0.43 bbl/min for Well #25. For Well #6, the relationship between pressure rise "ΔP" and volume of injected brine, V_B (i.e., the cavern compressibility for Well #6), as computed by Thiel and Russel, is βV = 1.29 bbls/psi (29.75 m^3/MPa) for a cavern volume V = 242,000 bbls (38,478 m^3). The cavern compressibility factor is β = 1.29/242,000 = 5.33 × 10^{-6}/psi or 7.7 × 10^{-4}/MPa. For Well #25, the cavern compressibility was measured as 0.47 bbls/psi (10.84 m^3/MPa) or in terms of cavern compressibility factor 3.7 × 10^{-6}/psi, or 5.4 × 10^{-4}/MPa. During the injection, the differential pressure between the brine side and the LPG side was relatively constant (hardly varied for Well #6 and varied less than 0.5 psi for Well #25), indicating the injected brine had a consistent specific gravity.

Figures 45 and 46 show the 3-day (72-hour) pressure histories (Pressure Observation data) following the test pressure increase, and Figures 47 and 48 reproduce the final 48 hours of the test periods. The slope of the pressure curves for both the brine and the LPG are used to calculate two apparent leak rates. For Well #6, the pressure loss rates determined by Thiel and Russel [2004] are –0.023 psi/hr on the LPG side and –0.015 psi/hr on the brine side based on the "hand-fit" slope of the pressure history in Figure 45. For a cavern compressibility of 1.29 bbl/psi, the computed leak rates are 260 bbls/year based on product pressure and 170 bbls/year based on brine pressure. For Well #25, the pressure loss rates were determined by Thiel and Russel [2004] as the difference between the pressure at time zero and at 72 hours averaged over the 72-hour period. The pressure drops were 3.23 psi for a rate of –0.045 psi/hr on the LPG side and a pressure drop of 2.27 psi for a rate of –0.035 psi/hr on the brine side. For a cavern compressibility of 0.47 bbl/psi, the computed leak rates are 185 bbls/year based on product pressure and 130 bbls/year based on brine pressure.

The test objective is to prove cavern integrity to within 1,000 bbls per year; for both wells and for both the brine pressure data and the product pressure data, the test objective is met. Moreover, the computed leak rates agree within less than 100 bbls per year whether using the product or brine pressure data.

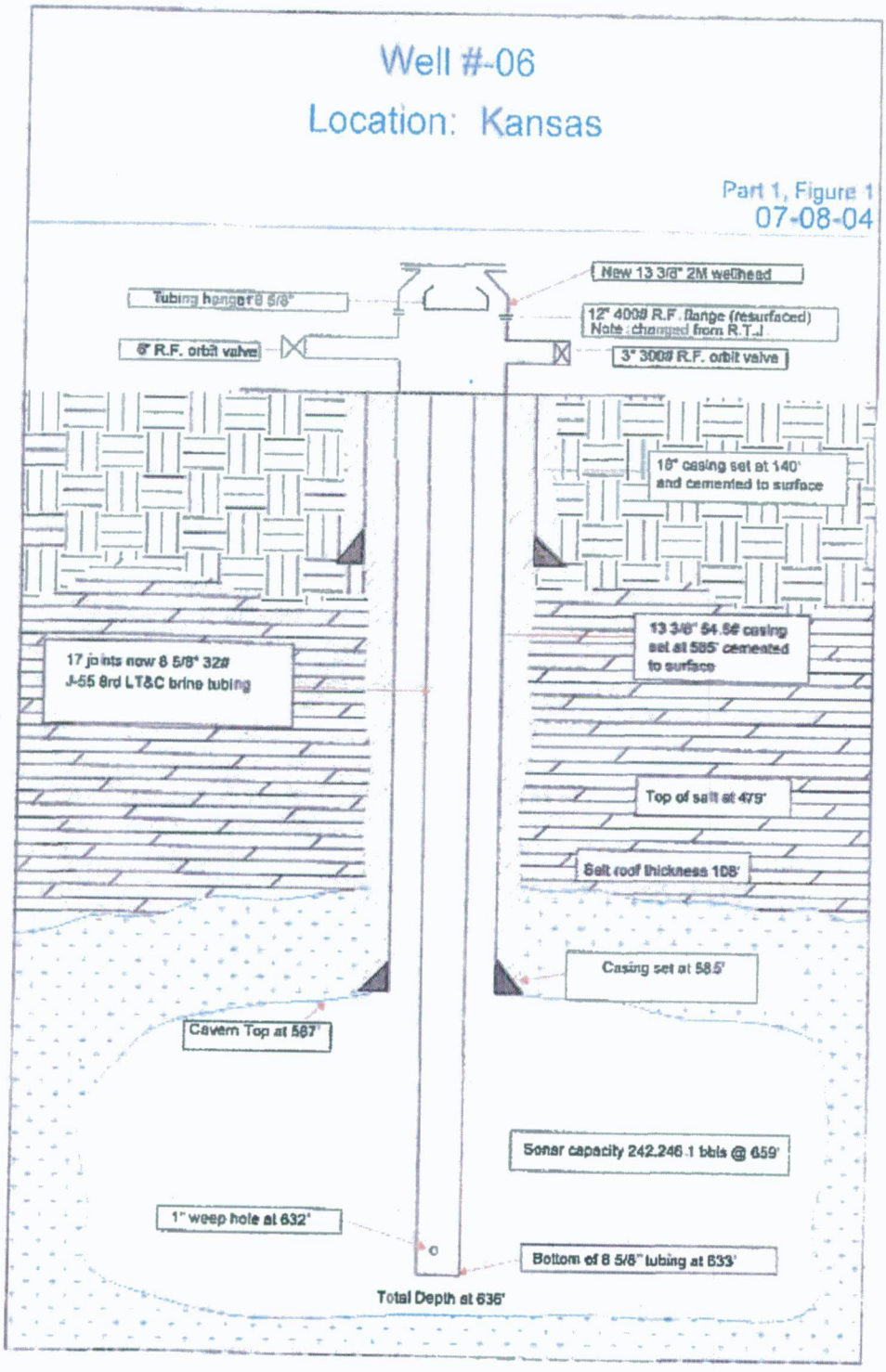

Figure 41. Kansas Well #6 Architecture.

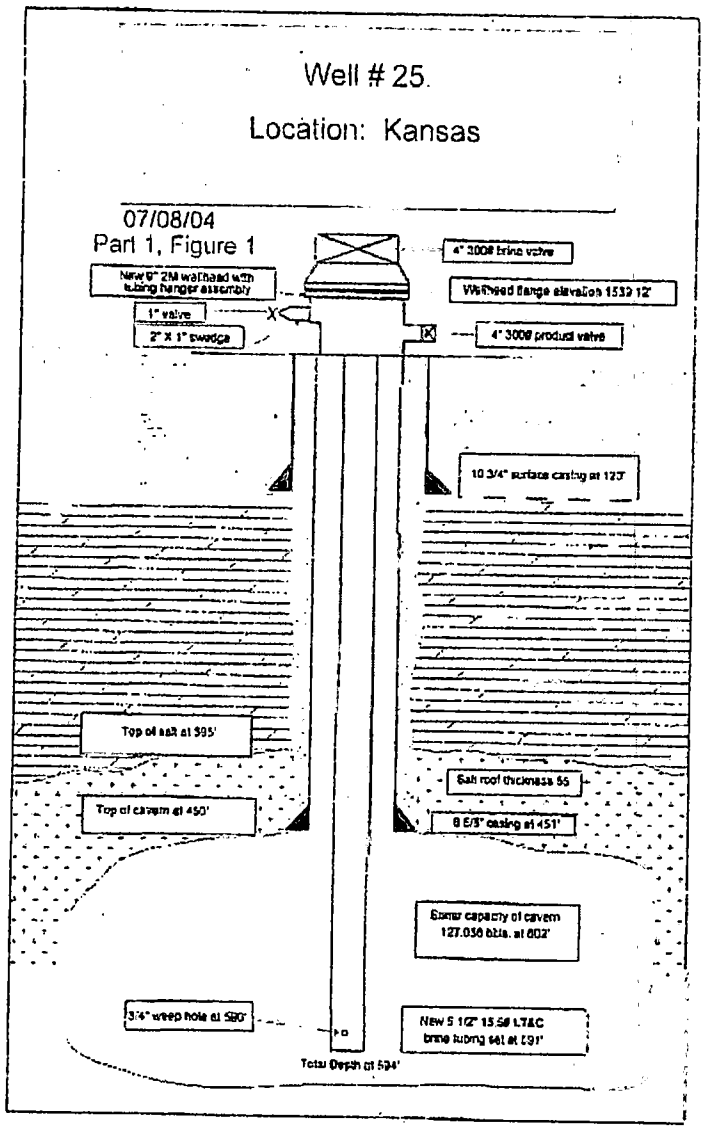

Figure 42. Kansas Well #25 Architecture.

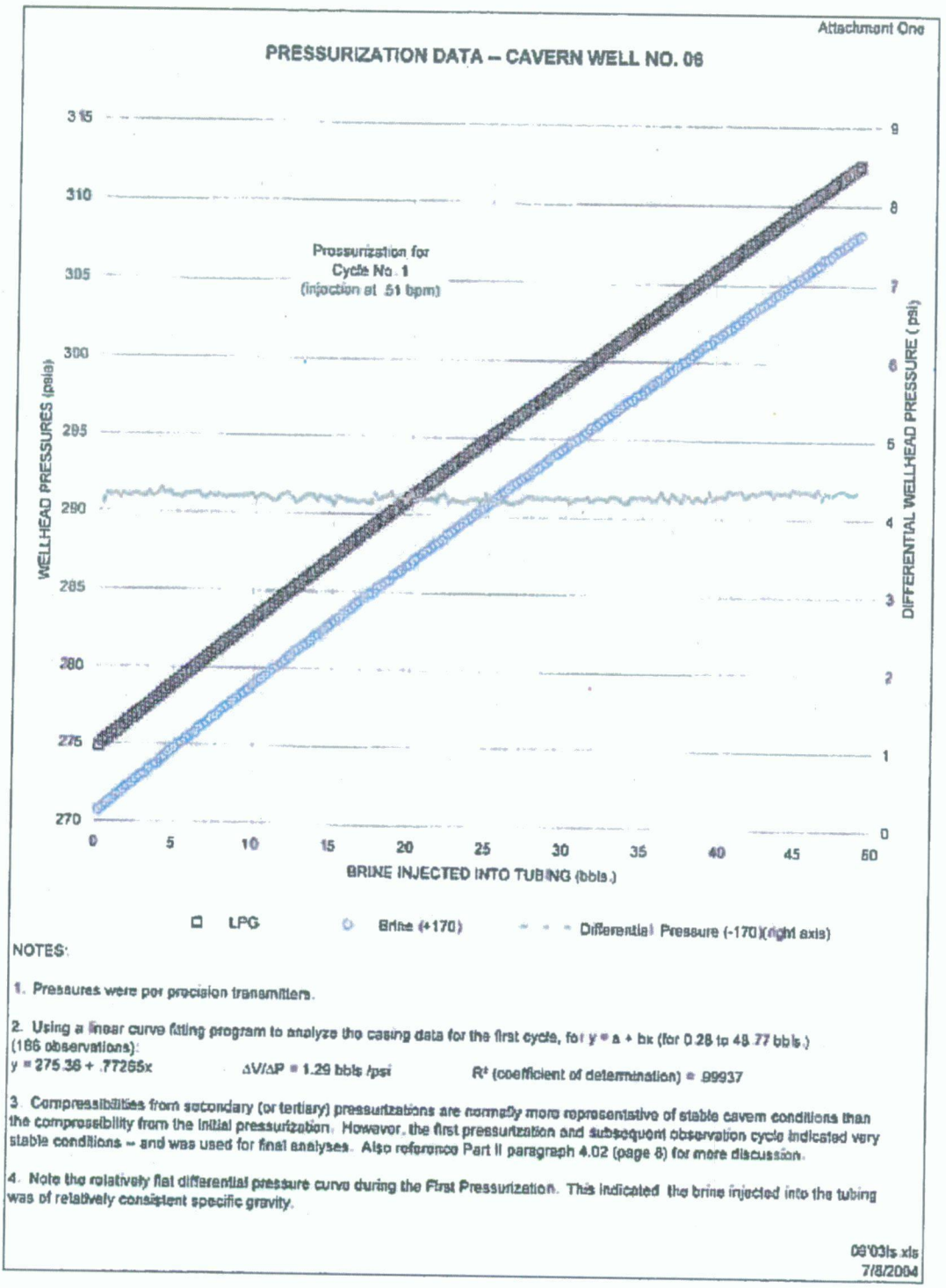

Figure 43. Kansas Well #6 Compressibility βV Measurement.

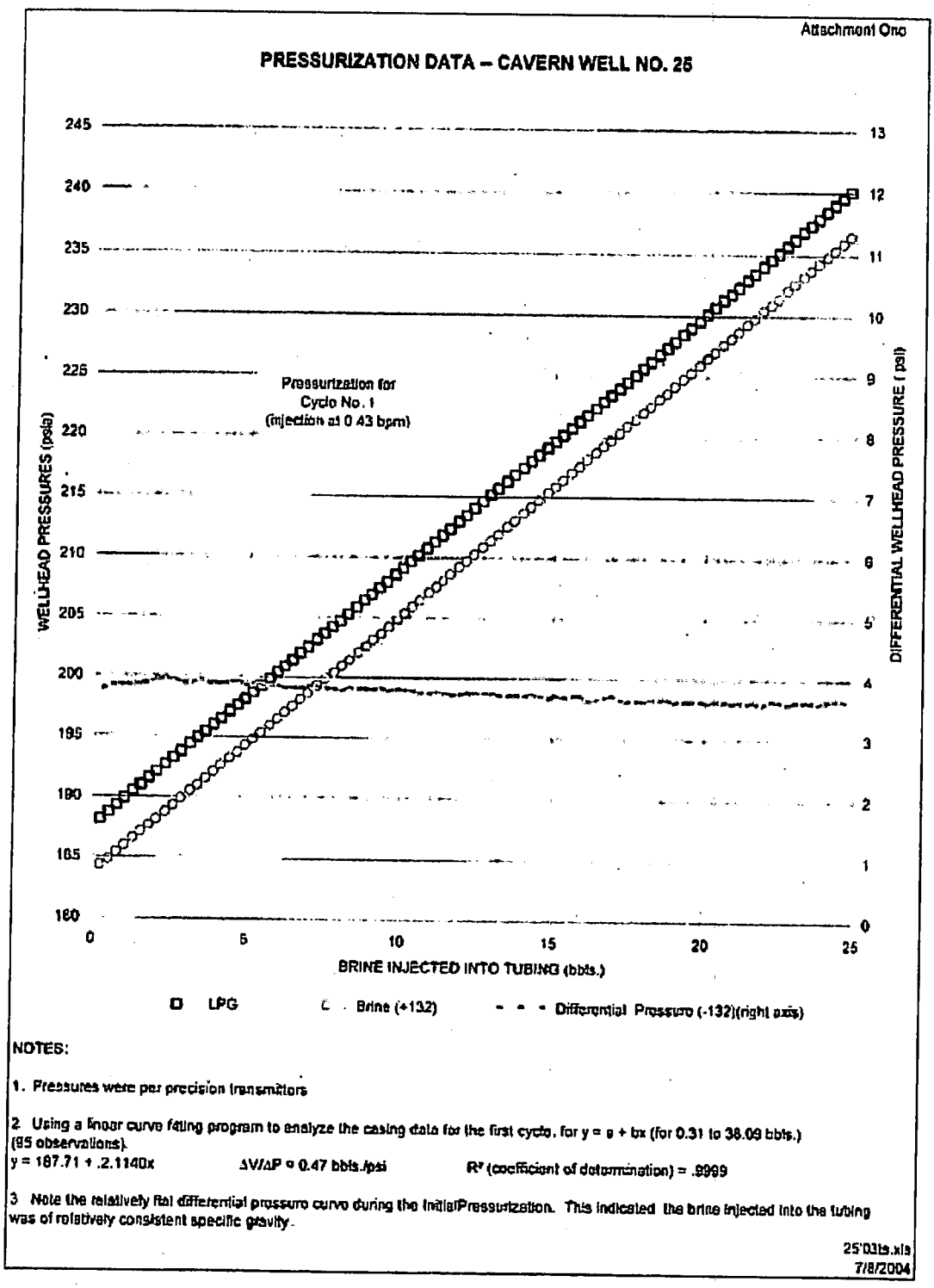

Figure 44. Kansas Well #25 Compressibility βV Measurement.

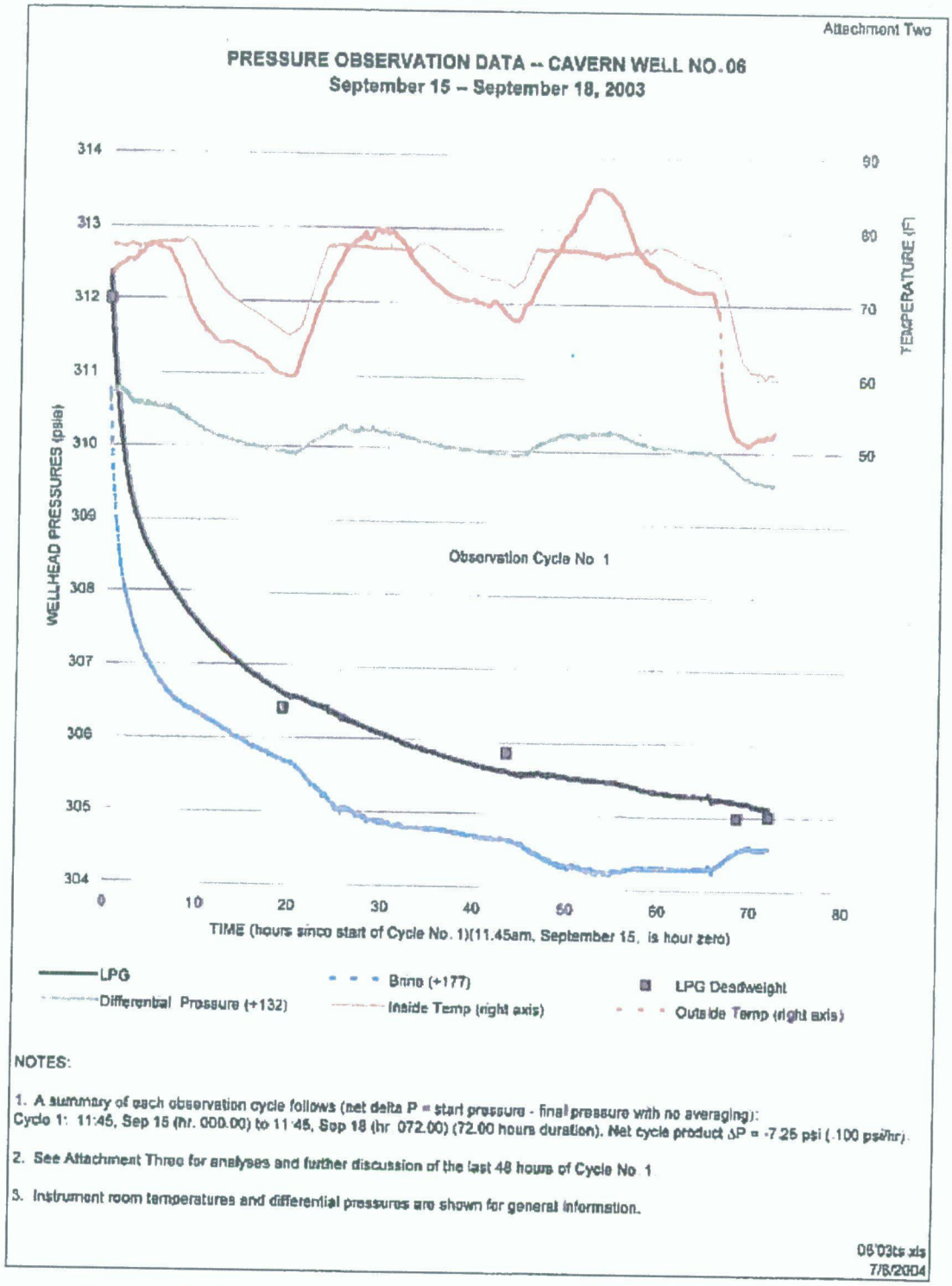

Figure 45. Kansas Well #6–Pressure Observation Data During a POT.

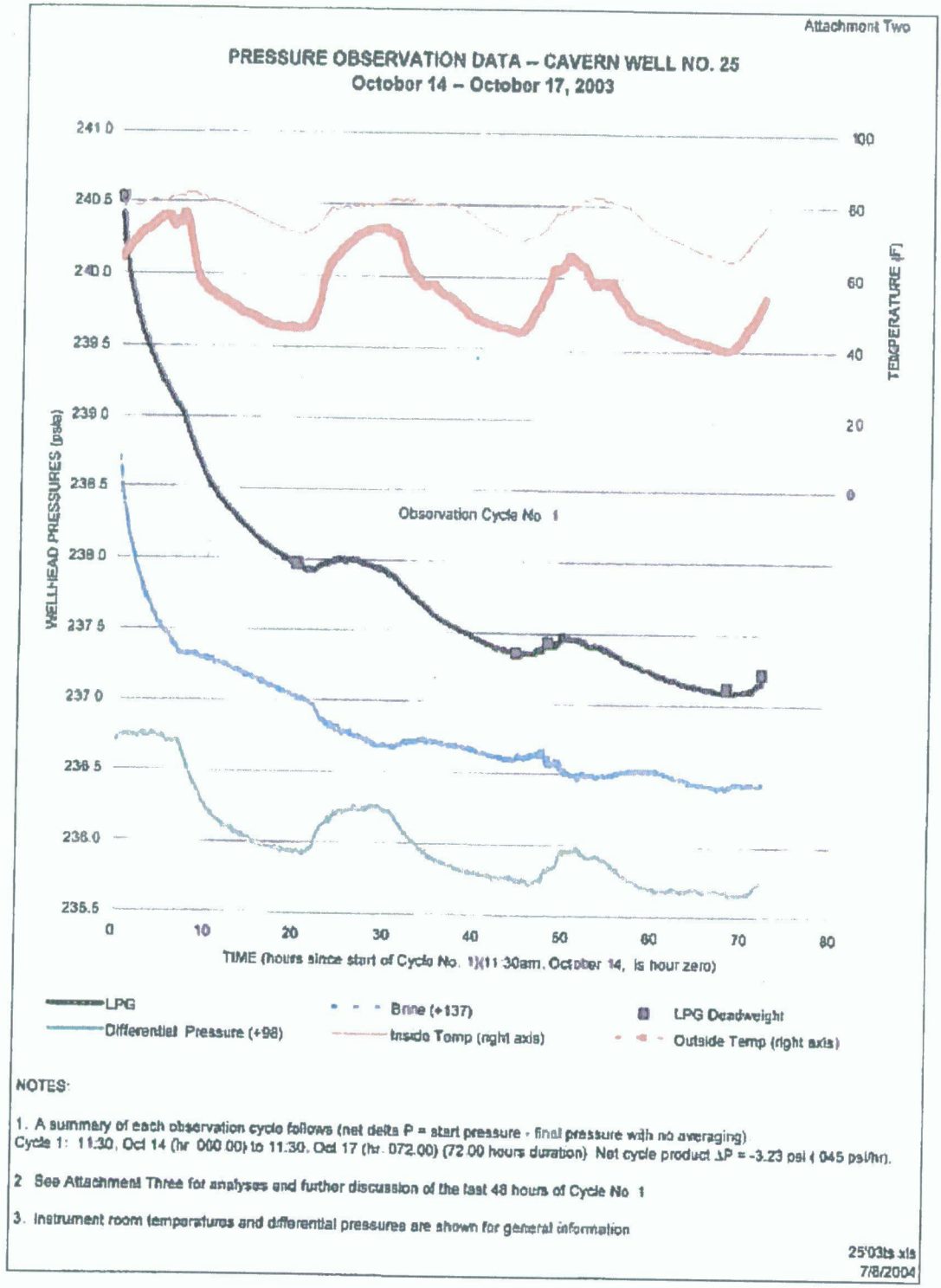

Figure 46. Kansas Well #25–Pressure Observation Data During a POT.

RSI-1476-05-051

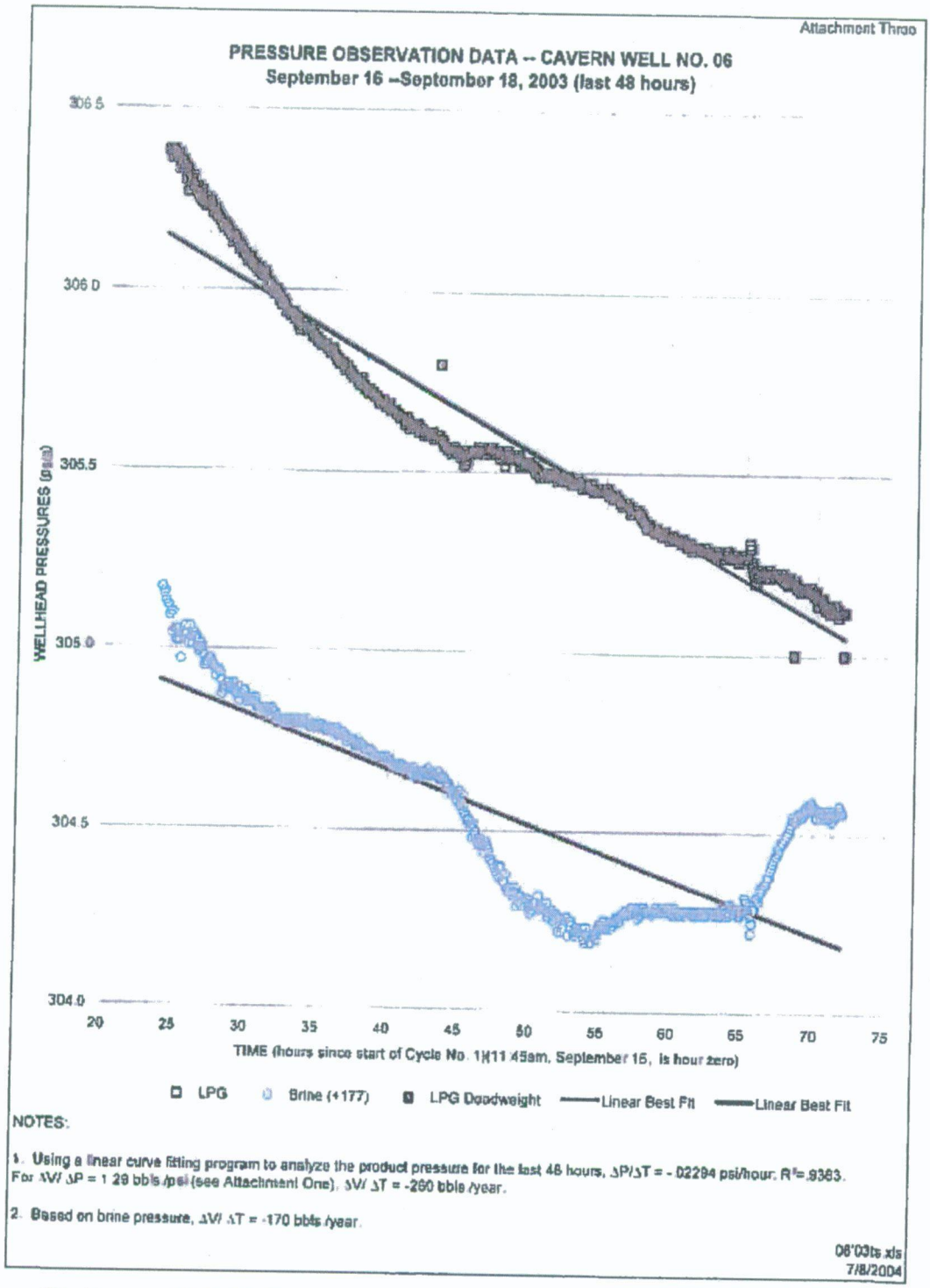

Figure 47. Kansas Well #6–Pressure Observation Data During the Last 48 Hours of a POT.

Attachment Three

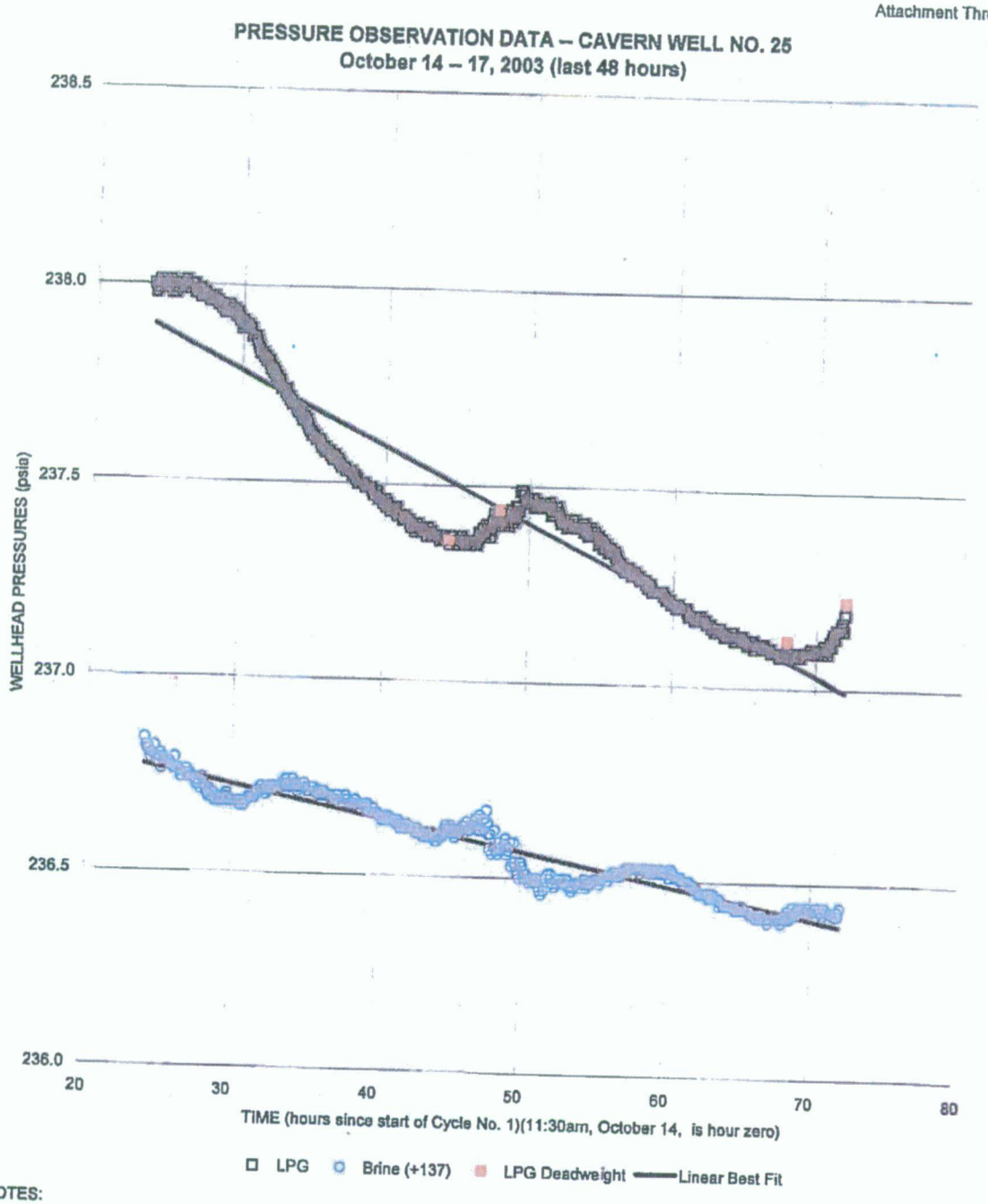

NOTES:

1. Using a linear curve fitting program to analyze the product pressure for the last 48 hours, $\Delta P/\Delta T$ = -.01890 psi/hour; R^2=.8916. For $\Delta V/\Delta P$ = 0.47 bbls./psi (see Attachment One), $\Delta V/\Delta T$ = -80 bbls./year.

2. Based on brine pressure, $\Delta V/\Delta T$ = -30 bbls./year.

25'03ts.xls
7/8/2004

Figure 48. Kansas Well #25–Pressure Observation Data During the Last 48 Hours of a POT.

12.9.2 Discussion of the Tests

The two Kansas cavern case histories studies warrant discussion about several of the testing considerations:

1. **Brine warming**

   As discussed in Section 6.3, brine warming is usually the single most important effect able to impair POT interpretation. Brine warming leads to an underestimation of the actual leak during a POT. However, for Kansas caverns, this effect is likely to be small. Typically, Kansas caverns vary in depth from 500 ft (150 m) to 1,000 ft (300 m); the difference between rock temperature at cavern depth and average ground temperature is small (a few °C), and even sometimes nil or negative (when brine ponds have been warmed in summer, injected brine may actually be somewhat warmer than the rock temperature at cavern depth). The depth of these two specific caverns is between 450 and 640 feet and the MITs were in September and October when the injected brine temperatures is most likely to be similar to the cavern temperature. For these reasons, brine warming can be discounted.

2. **Cavern compressibility**

   The as-measured cavern compressibilities for Caverns #6 and #25 are somewhat larger than would be expected based on sonar-measured cavern volumes. This discrepancy is believed to be common in bedded salt caverns. A compressibility greater than would be expected based strictly on the sonar volume of the cavern can be caused by (1) the flat shape of these caverns; (2) the large amount of insolubles/sediment at the cavern bottom, making the actual cavern volume significantly larger than the sonar cavern volume, and (3) the possible existence of "bells" or shale overhangs in which LPG was trapped during product removal–LPG compressibility is much larger than brine compressibility. Because the testers specifically measured the cavern compressibilities, no assumptions have to be made.

3. **Ground temperature variations**

   In the pressure histories, a strong correlation exists between pressure fluctuations (as a function of time) and outside air temperature. Such temperature-induced pressure variations are expected (see Section 6.2), and the correlations are more obvious when the pressure decay rate is slower. The ΔP-fluctuations are likely larger for a low heat-capacity fluid (LPG or nitrogen) in the annular space than for the brine in the inner tubing. The daily temperature cycle was consistent enough over the test period that simple subtraction of the pressures over a 48-hour or 72-hour interval could be used to resolve the temperature effects.

4. Salt Creep

An opinion expressed by Thiel and Russel [2004] is that the Kansas salt caverns do not exhibit measurable creep closure. One reason for this might be that the salt temperature is relatively low. Based on the average annual ground-surface temperature and a typical geothermal gradient for Kansas, the likely in situ salt temperature is in the vicinity of 60°F to 65°F. Indeed, cavern temperature logs in Kansas show that 63°F cavern temperatures are common, even for wells shut in for 2 years or more. A 63°F salt temperature is similar to temperatures experienced in the three underground Kansas salt mines. In the salt mines, salt creep certainly occurs as the pillars shorten with time, but the stresses imposed on the salt pillars are significantly greater than in the salt around the liquid-filled salt caverns. This aspect could be easily verified by a several week- or month-long collection of expelled brine from an open-wellhead of an inactive cavern. Cavern creep for these Kansas caverns compared to domal salt caverns can be compared using Equation (107). For the Kansas caverns, the depth and temperature are nominally 700 feet and 63°F (290 K). For domal salt caverns, the depth and temperature are nominally 2,500 feet and 145°F (336 K). The difference between the creep cavern closure is given by:

$$\frac{\dot{V}_{Kansas}}{\dot{V}_{domal}} = \left(\frac{depth_{Kansas}}{depth_{domal}}\right)^{n} \exp\left(-\frac{Q}{R}\left(\frac{1}{T_{Kansas}} - \frac{1}{T_{domal}}\right)\right)$$

For $n = 4$ and Q/R = 6,500 K (see Table 2):

$$\frac{\dot{V}_{Kansas}}{\dot{V}_{domal}} = \left(\frac{700}{2{,}500}\right)^{n} \exp\left(-6{,}500\left(\frac{1}{290} - \frac{1}{336}\right)\right) = 0.0003$$

The Kansas caverns will have considerably less creep than a domal salt cavern.

12.9.3 Interface Tests

The caverns in Kansas, because they are in a thin-bedded salt, simply do not have a neck suitable for an interface type-test–whether the interface measurement is made by wire-line logging or calculations using ΔP, the problem is the same. If one has a diameter at the product/brine (or nitrogen/brine) interface of 40 feet (for example), then a 0.25-foot (75 mm) interface movement over a 48-hour period equates to a minimum detectable leak rate of only 10,000 bbls per year. Greater test resolution is not possible for reasonable interface measurements.

By the same reasoning, Pressure Difference Observation tests are also unsuitable. In the Pressure Difference Observation test, the analysis of "ΔP" $\left(\Delta P = P_{ann}^{wh} - P_{tub}^{wh}\right)$, or the difference between the annular space (or LPG) wellhead pressure and the central tube (or brine) wellhead pressure is the focus of the tests. For the Kansas tests, ΔP decreases by about 0.3 psi when the

brine/hydrocarbon interface rises by 1 ft. Compared to the direct interface measurement discussed in the preceding paragraph, it would be even more difficult to obtain 0.25-foot resolution using ΔP data even with a long test period, which is unrealistic. Hence, the ΔP-method is suitable only when the cavern chimney is narrow and consistent, which is rare for bedded salt caverns compared to domal salt caverns.

Nonetheless, the Cavern #25 ΔP-evolution data can be interpreted as an example. At the computed interface location, the cross-sectional area, according to sonar survey, was 5–9 bbls/ft. Multiplying the cross-sectional area by the interface rise rate (for convenience say 1 ft/day based on a ΔP rate of 0.22 psi/day) yields a theoretical 5–9 bbls/day (about 2,000 bbls/yr) leak rate. Such a large leak rate is totally inconsistent with the measured wellhead pressure decay rates; the wellhead pressures would drop quickly with such a large leak rate.

12.9.4 Interface Location

The interface depth can be reasonably estimated from the differential pressure. For Well #6, the pressure difference is about 178 psi. If the pressure gradients are 0.52 psi/ft for brine and 0.22 psi/ft for LPG–a difference of 0.3 psi/ft, then the brine/LPG interface should be located at a depth of approximately 178/0.3 = 593 ft; i.e., or about 8 feet below the casing shoe, which is located at 585 ft. Bear in mind that a degree of uncertainty exists because of the inverse sensitivity of the calculated depth to the precision of the difference in pressure gradients between the brine and product. However, rudimentary estimates of the pressure gradients should allow estimates of the interface depth for standard LPGs (at these depths) within 5 feet.

Similarly, the tester should be able to predict or forecast the brine pressure that should be observed upon reaching a specific product wellhead pressure. Thiel and Russel (personal communication) feel such pretest brine-pressure predictions are within 1 or 2 psi for the Kansas caverns.

12.9.5 Casing Leaks

KDHE currently requires that the casing be tested (to a resolution of 100 bbls per year) separately from the cavern by using a packer in the tubing to conduct a hydraulic pressure test or nitrogen interface test. So far, KDHE has not accepted using wellhead product and brine pressure data (pressure difference monitoring) to prove casing integrity. The pressure difference testing method might, however, be a way to very accurately measure a product leak through the casing and through the casing shoe or to determine an internal leak from the annulus to the tubing. The test will be described in a hypothetical sense to illustrate the point.

Consider a test where the LPG/brine interface is located just above the casing shoe, say a few feet above, and the wellhead pressures are observed for a few hours. The pressure

difference evolution can distinguish between a leak from the casing shoe, Q_{cs}, and a leak through the casing, Q_{cas}. In theory, any difference in pressure decays observed in the tubing and in the annular space can be explained by a tiny leak from the casing to the tubing. If h_{tub} is the depth to the LPG/brine interface in the tubing, then

$$\frac{\Delta h_{tub}}{\Delta t} = \frac{1}{(\beta V \Delta\rho g + \Sigma + S)}\left[\left(\beta V + \frac{\Sigma}{\Delta\rho g}\right)\frac{\Delta P^{wh}_{tub}}{\Delta t} - \frac{\Sigma}{\Delta\rho g}\frac{\Delta P^{wh}_{ann}}{\Delta t}\right]$$

where $\Delta P^{wh}_{tub}/\Delta t$ is the brine pressure decay rate and $\Delta P^{wh}_{ann}/\Delta t$ is the produce pressure decay rate during the test, Σ is the annular cross section at interface depth, S is the tubing cross-sectional area, βV is the cavern compressibility, $\Delta\rho$ is the density difference between brine and LPG, and g is the gravitational acceleration.

Because Σ is much larger than $\beta V \Delta\rho g$, the pressure difference at the wellhead gives the velocity of the LPG/brine interface in the central tubing:

$$\frac{\Delta h_{tub}}{\Delta t} = \frac{1}{\Delta\rho g}\left[\frac{\Delta P^{wh}_{tub}}{\Delta t} - \frac{\Delta P^{wh}_{ann}}{\Delta t}\right]$$

Assume $\Delta p^{wh}_{tub}/\Delta t$ = –0.17 psi/day and $\Delta p^{wh}_{ann}/\Delta t$ = –0.45 psi/day, $\Delta\rho$ = 693 kg/m^3 and g = 9.8 m/sec^2, leading to $\Delta h_{tub}/\Delta t$ = 1 ft/day, which would be a very small leak, a few bubbles can explain the difference at wellhead.

Furthermore, this internal leak, Q_{int}, can be calculated :

$$Q_{int} = S_t \frac{\Delta h_{tub}}{\Delta t} = \frac{S_t}{\Delta\rho g}\left[\frac{\Delta P^{wh}_{tub}}{\Delta t} - \frac{\Delta P^{wh}_{ann}}{\Delta t}\right]$$

Assuming an S_t = 12.4 liters/meter tubing internal cross section, Q_{int} = 8.5 bbls/year. As the tubing pressure is about 99.4 psi (6.8 bars), it is very close to the vaporisation pressure of the LPG, so maybe the propane is in a gaseous state at the top of the tubing, and thus the mass of propane which has leaked is very small. It could be a good idea to performed the test at a slightly higher pressure in the tubing, say 150 psi; thus, in case of a internal leak, the LPG will stay in a liquid state in the tubing and it will be more easy to quantify this internal leak.

As the displacement of the LPG/brine interface in the cavern roof is negligible, the sum of the product leak through the casing, Q_{cas}, and the leak at casing shoe, Q_{cs}, can be directly deduced–and without approximation–from the annular pressure decay at the wellhead:

$$Q_{cas} + Q_{cs} = -\beta V \frac{\Delta P^{wh}_{ann}}{\Delta t} = -80 \text{ bbls/year}$$

As cavern compressibility is precisely measured, the product leak can be precisely calculated.

A second interpretation is that the brine pressure at the wellhead during the test was relatively low and close to LPG vaporization pressure. Even a tiny internal leak (i.e., LPG leaking from the annular space to the central space) could cause an inconsistent ΔP evolution, provided that the leaking LPG vaporizes when reaching the top of the brine-filled central tubing. Future consideration should be given to ensuring that the brine pressure at the wellhead in a POT is maintained higher than LPG vaporization pressure to avoid such an uncertainty.

13.0 CONCLUSIONS

In this chapter, the main conclusions from Chapters 5.0 through 9.0 are summarized. In these earlier chapters, several mechanisms contributing to the "apparent leak" were discussed. Their significance for the interpretation of an MIT is summarized in this chapter.

Two generic types of MIT are considered:

- In the Liquid-Liquid Interface tests (POT and PDO), the cavern contains no gas; the main interest is in the liquid pressure evolution, which is measured at the wellhead.
- In the Gas-Liquid Interface tests (NIT), it is assumed that the gas-liquid interface (usually nitrogen-brine interface) is located where the horizontal cross-sectional area is small (a few square meters or less). In such a case, the main interest is in the rate of interface movement, which is equal to the apparent gas volume loss divided by the cross-sectional area at interface depth.

13.1 PREEXISTING TEST PHENOMENA

Cavern characteristics that may exist before LLI and NIT tests are conducted include:

1. Steady-state brine permeation is exceedingly small.
2. The effects of daily ground temperature variations are difficult to predict. These temperature variations generate daily wellhead pressure changes ranging from ±500 Pa (one tenth of a psi) to ±10 kPa (1 psi). Time lags often are observed. However, these variations can be partly neutralized by analyzing 24-hour increments (i.e., comparing pressures at the same time of day).
3. The effects of well temperature variation (temperature change between the ground surface and the casing shoe) are negligible, provided that the well has been kept idle for almost a couple of days before the test is performed.
4. Steady-state creep is often very small, except when the cavern is very deep (say, deeper than 1,500 m or 5,000 ft). In fact, steady-state and transient creep must be assessed together (see below).
5. Effects induced by cavity brine warming are significant in most cases (an exception is the case of very shallow caverns). They depend on cavern size, initial temperature difference (for instance, as it is at the end of the leaching phase), and time elapsed since leaching was completed. When an LLI is considered, the largest pressure increase rates caused by thermal expansion are achieved when (1) the cavern is small; (2) the initial temperature difference between brine and ambient rock temperature is large; and/or

(3) the elapsed time, t, since leaching (or since last product removal) is short. When V = 8,000 m^3, $\bar{\theta}_R - \theta_I(0)$ = 18.5°C (initial temperature gap), t = 1–3 months, a typical rate of pressure increase in an LLI, generated by thermal expansion, is 0.06 MPa/day (8 psi/day). In this example, the actual leak (directly deduced from wellhead pressure evolution) would be underestimated by 240 liters/day (1.5 bbls/day).

When an NIT test is considered, brine warming results in interface rise; the actual leak is overestimated. Even if the test is conducted a couple of years after leaching is completed, the actual leak (directly deduced from gas-liquid interface rate) will be overestimated.

13.2 PHENOMENA TRIGGERED BY THE TESTS

The phenomena triggered by MITs are as follows:

1. **Adiabatic compression:** The consequences of the small adiabatic brine temperature increase generated by a rapid pressure increase are small except during a short period after the increase (1–2 days).

2. **Transient creep:** Transient creep that results in an increase in cavern volume and a decrease in brine pressure is a relatively slow phenomenon. The effect of transient creep is more difficult to assess precisely than the effect of most other phenomena, because transient creep is a nonlinear function of the initial rock mass temperature and cavern pressure, and of the intensity of the MIT pressure increase.

3. **Transient micropermeation:** The effect of transient permeation through the rock mass is larger when the cavern is small and the permeability is large. However, even when a somewhat extreme case is considered (V = 8,000 m^3, $K_{salt}^{hyd} = 10^{-19}$ m^2, $\phi = 10^{-2}$), the pressure drop in a POT is 0.4 percent of the initial pressure increase 1 day after pressurization is completed and 0.8 percent of the initial pressure increase 4 days after pressurization is completed.

4. **Additional dissolution:** Additional salt dissolution results in a delayed pressure drop. The overall pressure drop is 4.3 percent of the initial pressure increase. For example, when the initial pressure increase is 5 MPa (700 psi), the pressure drop in an LLI resulting from additional dissolution is 0.215 MPa (31 psi). This pressure drop seems to be a relatively slow phenomenon lasting approximately 10 days in an 8,000-m^3 cavern. However, the pressure drop rate is much faster during the first and second days immediately following the pressurization. This process is probably longer in larger caverns.

When an LLI is considered, all these phenomena lead to an overestimation of the actual leak.

13.3 BRINE WARMING CONCLUSIONS

Brine warming (a preexisting test condition), transient creep, and additional transient dissolution (triggered by the test) are the most important mechanisms influencing MIT results.

13.3.1 Conclusions for an LLI

During an LLI, brine warming leads to an underestimation of the leak. In the case of some shallow caverns, the reverse (brine cooling) can lead to overestimation of the leak. The effect of brine warming can, in some caverns, be assessed by performing a shut-in pressure test before the MIT.

Additional dissolution and transient creep (and to a smaller extent, adiabatic pressure increases) lead to an overestimation of the actual leak. These mechanisms can readily be eliminated by providing a long enough "stabilization period" after the cavern has been pressurized to its final pressure. A 5-day stabilization period is recommended, but a 10-day stabilization period would be better. Such a long period is costly, but the benefit is that the observed leak will be closer to the actual leak and, incidentally, significantly smaller than the leak observed when there is no stabilization period. Many testing companies manage such a stabilization period during an MIT.

13.3.2 Conclusions for an NIT

During an NIT, brine warming leads to an overestimation of the leak; additional dissolution and transient creep (and to a smaller extent, adiabatic pressure increases) lead to an underestimation of the leak.

13.4 USEFUL RELATIONS

13.4.1 Estimations of Cavern Volume Change Rates

The formulae presented apply to a spherical cavern,[6] radius R. In some cases, the formulae for a cylindrical cavern, radius R, also are given. Quantities such as Q/V are positive.

- **Steady-state permeation**

$$\frac{Q_{perm}^{ss}}{V} = \frac{3K_{salt}^{hyd}}{\mu_b R^2} p_i^1 \tag{143}$$

[6] There is no closed-form solution in the case of a cylinder.

Q_{perm}^{ss} = steady-state permeation flow (m^3/s)

K_{salt}^{hyd} = rock salt intrinsic permeability (10^{-22} to 10^{-19} m^2)

μ_b = brine viscosity ($1.2 \cdot 10^{-9}$ MPa·s)

R = cavern radius (m)

V = cavern volume (m^3)

p_i^1 = initial pressure build-up (MPa)

- **Steady-state creep**

  - Sphere

$$\frac{Q_{creep}}{V} = \frac{3}{2}\left[\frac{3}{2n}\left(P_\infty - P_o - p_i^1\right)\right]^n A \cdot \exp\left(-\frac{Q}{\Re T_R^\infty}\right) \tag{144}$$

  - Cylinder

$$\frac{Q_{creep}}{V} = \sqrt{3}\left[\frac{\sqrt{3}}{n}\left(P_\infty - P_o - p_i^1\right)\right]^n A \cdot \exp\left(-\frac{Q}{\Re T_R^\infty}\right) \tag{145}$$

Q_{creep} = steady-state creep flow (m^3/s)

P_∞ = geostatic pressure (MPa)

P_o = halmostatic pressure (MPa) for an open cavern or the cavern pressure for a closed cavern

p_i^1 = initial pressure build-up (MPa)

A, $Q/\Re$, n = creep parameters (see Table 2)

T_R^∞ = absolute temperature at cavern depth (K)

- **Brine warming**

Must be computed (or measured) on a case-by-case basis. However, when the cavern is roughly spherical or cylindrical and has been freshly washed out or emptied of product (more precisely, if $t < t_c^{th} = R^2/\pi k_{salt}^{th}$, where t is the time after wash out was completed), the following approximations can be used:

  - Sphere

$$\frac{Q_{th}}{V} = \frac{3\chi\alpha_b}{R}\left[\theta_R^\infty - \theta_f(0)\right]\sqrt{\frac{k_{salt}^{th}}{\pi t}} \simeq \frac{1.68 \cdot 10^{-4}}{R\,(\text{m})}\left[\theta_R^\infty - \theta_f(0)\right]\frac{1}{\sqrt{t\,(\text{days})}} \tag{146}$$

- Cylinder

$$\frac{Q_{th}}{V} = \frac{2\chi\alpha_b}{R}\left[\theta_R^{\infty} - \theta_l(0)\right]\sqrt{\frac{k_{salt}^{th}}{\pi t}} \approx \frac{10^{-4}}{R\,(\text{m})}\left[\theta_R^{\infty} - \theta_l(0)\right]\frac{1}{\sqrt{t\,(\text{days})}} \tag{147}$$

However, when t is not much smaller than t_c^{th}, these approximations overestimate the effect of brine warming.

Q_{th} = brine flow (m^3/s)

α_b = brine thermal expansion coefficient ($\alpha_b = 4.4 \cdot 10^{-4}$/°C)

$\theta_R^{\infty} - \theta_l(0)$ = initial temperature gap (°C)

χ = thermal capacities ratio ($\chi = 4/9$ when brine and salt are considered)

k_{salt}^{th} = salt thermal diffusivity ($k_{salt}^{th} = 3 \cdot 10^{-6}$ m^2/s)

- **Brine cooling following adiabatic pressure increase**

  - Sphere

$$\frac{Q_{ad}}{V} = \frac{3\chi\alpha_b}{R}\left[\frac{\alpha_b T_l}{\rho_b C_b^p}\right] p_l^1 \sqrt{\frac{k_{salt}^{th}}{\pi t}} \approx \frac{4.8 \cdot 10^{-6}}{R\,(\text{m})} \frac{p_l^1\,(\text{MPa})}{\sqrt{t\,(\text{days})}} \tag{148}$$

  - Cylinder

$$\frac{Q_{ad}}{V} = \frac{2\chi\alpha_b}{R}\left[\frac{\alpha_b T_l}{\rho_b C_b^p}\right] p_l^1 \sqrt{\frac{k_{salt}^{th}}{\pi t}} \approx \frac{3.6 \cdot 10^{-6}}{R\,(\text{m})} \frac{p_l^1\,(\text{MPa})}{\sqrt{t\,(\text{days})}} \tag{149}$$

Q_{ad} = brine flow (m^3/s)

T_l = brine (absolute) temperature (K)

ρ_b = brine density (1,200 kg/m^3)

C_b^p = brine heat capacity ($C_b^p = 3{,}800$ J/kg-°C)

p_l^1 = initial pressure increase (MPa)

- **Transient creep**

No simple approximation is available. Computations have to be performed on a case-by-case basis.

- **Transient permeation**

  If t is the time after the pressure increase, when $t < t_c^{hyd} = \mu_b \phi \beta' R^2 / \pi K_{salt}^{hyd}$, the following approximation can be used:

  – Sphere

$$\frac{Q_{perm}^{tr}}{V} = Q_{perm}^{ss} \cdot \left(1 + \sqrt{t_c^{hyd} / t}\right) \tag{150}$$

  – Cylinder

$$\frac{Q_{perm}^{tr}}{V} = \frac{K_{salt}^{hyd}}{\mu_b R^2}\left(1 + 2\sqrt{t_c^{hyd} / t}\right) \tag{151}$$

Q_{perm}^{tr} = transient micro-permeation flow (m^3/s)

Q_{perm}^{ss} = steady-state micropermeation flow (m^3/s), see Equation (143) for spherical cavern

ϕ = rock salt porosity ($\phi = 0.002$ to 0.01)

β' = salt matrix compressibility factor ($\beta' - \beta \approx 4 \cdot 10^{-4}$ /MPa)

K_{salt}^{hyd} = rock salt intrinsic permeability (10^{-22} to 10^{-19} m^2)

μ_b = brine dynamic viscosity ($1.2 \cdot 10^{-9}$ MPa·s)

- **Additional dissolution**

$$\frac{Q_{diss}}{V} = 0.043 \frac{\beta}{t_c^{diss}} p_i^1 \cdot \exp(-t / t_c^{diss}) \tag{152}$$

Q_{diss} = cavern volume increase minus brine volume decrease (m^3/s)

β = cavern compressibility factor ($\beta = 4 \cdot 10^{-4}$ /MPa is typical)

t_c^{diss} = dissolution characteristic time (t_c^{diss} is a few days for small caverns and greater for large caverns)

p_i^1 = initial pressure increase (MPa)

13.4.2 Brine or Cavern Volume Changes

Let Q (in m^3/s or bbl/s) be the brine or cavern volume change rate caused by phenomena such as transient creep, additional dissolution, and thermal expansion.

$$Q = Q_{cr}^{ss} - Q_{cr}^{tr} + Q_{th} - Q_{th}^{ad} - Q_{perm}^{tr} - Q_{diss} \tag{153}$$

Let Q^* be an estimation of Q.

13.4.3 Relation Between Tubing Pressure Variation and Apparent Leak in an LLI Test

The pressure decay rate $\dot{P}_{tub}^{wh}$ as measured at the top of the tubing during a POT is linked to the preexisting and triggered phenomena by the following relation:

$$-\frac{Q_{app}}{\beta V} = \dot{P}_{tub}^{wh} = \frac{Q - Q_{leak}}{\beta V} \tag{154}$$

13.4.4 Relation Between Actual Leak and Apparent Leak in an NIT

During an NIT, the theoretical leak Q_{leak} is linked to the apparent leak Q_{app} and to the preexisting and triggered phenomena by the following relation:

$$Q_{app} \cdot \left(\frac{1}{\beta V} + \frac{1}{\beta_g V_g^o} \right) = \frac{Q_{leak}}{\beta_g V_g^o} + \frac{Q}{\beta V} \tag{155}$$

where $Q_{app} = -\Sigma \dot{h}$, $\dot{h}$ is the interface rate, and Σ is the cross-sectional area at interface depth.

13.4.5 Relation Between Actual Leak and Corrected Leak in an LLI Test

During a POT, the corrected leak Q_{leak}^{corr} is linked to the apparent leak Q_{app} and to the estimation Q^* of the phenomena, which change the cavern or brine volume, by the following relation:

$$Q_{leak}^{corr} = Q^* + Q_{app} = Q^* - \beta V \cdot \dot{P}_{tub}^{wh} \tag{156}$$

13.4.6 Relation Between Actual Leak and Corrected Leak in an NIT

During an NIT, the corrected leak Q_{leak}^{corr} is linked to the apparent leak Q_{app} and to the estimation Q^* of the phenomena, which change the cavern or brine volume, by the following relation:

$$Q_{leak}^{corr} = -\frac{\beta_g V_g^o}{\beta V} \cdot Q^* + \left(1 + \frac{\beta_g V_g^o}{\beta V} \right) \cdot Q_{app} \tag{157}$$

14.0 NOMENCLATURE

Symbol	Parameter	Unit
A	Parameter of Norton-Hoff steady-state creep law	/Pa^n–s
a,b	Half-axis of a spheroidal cavern	m
a_s	Parameter for the calculation of saturated brine density	/Pa
α	Liquid thermal-expansion coefficient	/°C
α_b	Brine thermal-expansion coefficient	/°C
α_l	Liquid thermal-expansion coefficient	/°C
α_o	Oil thermal-expansion coefficient	/°C
α_ω	Parameter of Munson creep law	—
b_s	Parameter for the calculation of saturated brine density	/°C
β	Cavern compressibility factor	/Pa
β'	Rock-matrix compressibility factor	/Pa
β_b	Brine compressibility factor	/Pa
β_b^{ad}	Brine adiabatic-compressibility factor	/Pa
β_c	Cavern compressibility factor	/Pa
β_E	Cavern elasticity	/Pa
β_g^{ad}	Gas adiabatic-compressibility factor	/Pa
β_g^{int}	Gas compressibility factor at gas/brine interface	/Pa
β_g^{isoth}	Gas isothermal-compressibility factor	/Pa
β_h	Hydrocarbon compressibility factor	/Pa
β_{LPG}^{ad}	LPG adiabatic compressibility factor	/Pa
β_{prop}	Propane compressibility factor	/Pa
β_{prop}^{ad}	Propane adiabatic-compressibility factor	/Pa
$\beta_g V_g^o$	Compressibility of a nitrogen column	m^3/Pa
β_ω	Parameter of Munson creep law	—
βV	Cavern compressibility	m^3/Pa
C	Correction parameter for barometric effect during NIT	—

Symbol	Parameter	Unit
C_b^p	Brine heat capacity at constant pressure	J/kg–°C
C_f^p	Fluid heat capacity at constant pressure	J/kg–°C
C_l^p	Liquid heat capacity at constant pressure	J/kg–°C
C_g	Gas heat capacity	J/kg–°C
C_{liq}	Liquid heat capacity	J/kg–°C
C_{salt}	Salt heat capacity	J/kg–°C
c	Brine concentration	—
c_b	Speed of sound in brine	m/s
c_{LPG}	Speed of sound in LPG	m/s
c_{prop}	Speed of sound in propane	m/s
c_{ref}	Reference concentration for saturated brine	—
c_{sat}	Saturated brine concentration	—
c_{sat}^f	Brine salt saturation (finish value)	—
c_{sat}^o	Brine salt saturation (starting value)	—
χ	Ratio of salt and liquid volumetric heat capacity	—
$\delta\varepsilon$	Change in rock strain (e.g., earth tides)	—
δh	Interface displacement	m
δM_b	Additional mass of saturated brine	kg
δP^{wh}	Wellhead pressure change	Pa
δP_{ann}^{wh}	Variation of annular pressure at wellhead	Pa
δP_l	Cavern pressure variation	Pa
δP_{tub}^{wh}	Variation of central tubing pressure at wellhead	Pa
δP_{wh}	Wellhead pressure increase	Pa
$\delta\rho_b$	Brine density difference or variation	kg/m^3
$\delta\rho_{liq}$	Liquid density variation	kg/m^3
$\delta\theta_{av}$	Variation of the average temperature in the well	°C
δV	Cavern volume increase	m^3
δV_b	Brine volume variation in the cavern	m^3
δV_{inj}	Volume of liquid injected at wellhead	m^3

Symbol	Parameter	Unit
δV_{perm}	Volume of brine expelled from the cavern by permeation	m^3
δv	Volume change of liquid because of temperature change	m^3
Δ	Laplacian operator	—
γ	Gas compressibility empirical factor	—
ξ	Parameter for calculation of the heating of a spherical cavern	—
ζ	Internal variable of Munson creep law	—
E	Young's modulus of salt	Pa
e	Relative error for cavern compressibility measurement	—
$erfc$	Complementary error function	—
ϕ	Rock mass porosity	—
Φ	Ratio of well volume below casing shoe to cavern volume	—
ε	Cavern relative volume change	—
ε_t^*	Parameter of Munson creep law	/s
$\dot{\varepsilon}_{ss}$	Sample steady-state height reduction rate	/s
$\dot{\varepsilon}_{creep}^{ss}$	Steady-state creep rate of a cavern	/s
F	Parameter of Munson creep law	—
f	Shape factor for compressibility factor calculation	—
φ	Shape factor for thermal heating calculation	—
G^{th}	Average geothermal gradient	°C/m
g	Gravitational acceleration	m^2/s
H	Cavern average depth	m
H_{cs}	Casing seat depth	m
h	Depth of brine/nitrogen or brine/hydrocarbon interface	m
h	Also used for hours	
$\hbar$	Insoluble layer thickness	m
h_i	Depth of injected brine/saturated-brine interface	m
h_{int}^o	Depth to gas/brine interface	m
h_l	Movement of an interface	m
h_{tub}	Central tube length	m

Symbol	Parameter	Unit
h^1	Initial interface position (height)	m
h^f	Final interface position (height)	m
K_o	Parameter of Munson creep law	—
K^{hyd}	Intrinsic hydraulic permeability	m^2
K_{salt}^{hyd}	Salt intrinsic permeability	m^2
K_{salt}^{th}	Salt thermal conductivity	W/m–°C
k_{gr}^{th}	Ground thermal diffusivity	m^2/s
k_{salt}^{hyd}	Salt hydraulic conductivity	m^2/s
k_{salt}^{th}	Salt thermal diffusivity	m^2/s
κ	Parameter for the calculation of saturated brine concentration with temperature change	/°C
l	Length of a cylinder	m
λ	Gas pressure constant	m^3/ kg-MPa
$\hat{\lambda}$	Salt dissolution-induced pressure change	/MPa
M_b	Cavern brine mass	kg
m	Parameter of Munson creep law	—
m_g	Mass of gas in the annular space	kg
μ	Dynamic viscosity	Pa·s
μ_b	Dynamic viscosity of brine	Pa·s
μ_g	Dynamic viscosity of nitrogen	Pa·s
μ_{LPG}	Dynamic viscosity of LPG	Pa·s
μ_{oil}	Dynamic viscosity of oil	Pa·s
n	Parameter of Norton-Hoff steady-state creep law	—
ν	Poisson's ratio	—
ω	Pulsation of atmospheric-temperature variations	/s
P_{ann}^{wh}	Annular pressure at wellhead	Pa
P_o	Halmostatic pressure	Pa
P_g	Gas absolute pressure at interface depth	Pa
P_g^{int}	Gas pressure at gas/brine interface	Pa

Symbol	Parameter	Unit
P_g^{wh}	Gas pressure at wellhead	Pa
P_b^{wh}	Brine pressure at wellhead	Pa
P_l	Average pressure in the cavern	Pa
P_l^0	Cavern pressure before injection	Pa
P_l^1	Cavern pressure immediately after injection	Pa
P_l^f	Final cavern pressure after some decay	Pa
p_l^f	Pressure increment (after decay)	Pa
p_l^1	Pressure increment immediately after change	Pa
P_{pore}	Pore pressure	Pa
P_{ref}	Pressure reference for the calculation of saturated brine density and concentration	Pa
P_{tub}^{wh}	Central tubing pressure at wellhead	Pa
P_{-}	Geostatic earth pressure	Pa
p	Difference between actual pore pressure and halmostatic pressure	Pa
p_l	Difference between actual cavity pressure and halmostatic pressure	Pa
Φ	Fraction of permeation area	—
Ψ	Parameter for the calculation of saturated brine concentration	/Pa
ϕ	Rock mass porosity	—
Q	Cavern or brine volume change rate caused by such phenomena as brine thermal expansion, salt creep etc.	m^3/s
Q^*	Estimation of Q	m^3/s
$Q/\Re$	Parameter of Norton-Hoff steady-state creep law	K
Q_{app}	Apparent leak rate	m^3/s
Q_{cas}	Leak rate through casing	m^3/s
Q_{cs}	Leak rate through casing shoe	
Q_{dlss}	Cavern volume change rate caused by dissolution	m^3/s
Q_{leak}	Actual hydrocarbon leak rate	m^3/s
Q_{perm}	Leak rate because of permeation	m^3/s

Symbol	Parameter	Unit
Q_{tub}	Leak rate through tubing	m^3/s
Q_{leak}^{corr}	Corrected hydrocarbon leak rate	m^3/s
Q_{perm}^{tr}	Transient micropermeation flow rate	m^3/s
Q_b^{wh}	Brine leak at the wellhead	m^3/s
Q_{cr}^{ss}	Cavern volume change rate–steady-state creep	m^3/s
Q_{cr}^{tr}	Cavern volume change rate–transient creep	m^3/s
Q_{perm}^{ss}	Steady-state micropermeation flow rate	m^3/s
Q_{th}	Brine outflow rate because of thermal expansion	m^3/s
Q_{th}^{ad}	Brine outflow rate because of cooling after pressure build-up	m^3/s
Q_{diss}^{NLT}	Apparent leak rate in NIT by dissolution	m^3/s
q_{heat}^{ad}	Heat flux across cavern wall–adiabatic warning	w
q_{ad}^{ss}	Heat flux from spherical cavern–adiabatic warning	w
R	Radius of spherical cavern	m
r	Radial coordinate	m
r_g	Gas-specific constant	$m^2/s–K$
ρ	Density (mass per unit volume)	kg/m^3
ρ_b	Brine density	kg/m^3
ρ_n	Nitrogen density	kg/m^3
ρ_{oil}	Oil density	kg/m^3
ρ_{sat}^0	Brine density (saturated) before pressure change	kg/m^3
ρ_{sat}^f	Brine density (saturated) after pressure change	kg/m^3
ρ_b^{ref}	Density reference for the calculation of saturated brine density	kg/m^3
ρ_b^{sat}	Saturated brine density	kg/m^3
ρ_f	Fluid density	kg/m^3
ρ_g	Gas density	kg/m^3
ρ_h	Hydrocarbon density	kg/m^3
ρ_{liq}	Liquid density	kg/m^3

Symbol	Parameter	Unit
ρ_{prop}	Propane density	kg/m^3
ρ_{salt}	Salt density	kg/m^3
S	Surface area of the cavern wall	m^2
S_a	Average cross-section area of a well	m^2
S_t	Central tubing cross-sectional area	m^2
S_w	Cross-sectional area of the well	m^2
s	Cross section of a long cylinder	m^2
Σ	Annular space cross-section at interface depth	m^2
σ	Axial stress applied during an uniaxial test	Pa
T	Absolute temperature	K
T_R^-	Absolute temperature of the salt	K
t	Time	s
t_c^{diss}	Dissolution characteristic time	s
t_c^{hyd}	Hydraulic characteristic time	s
t_c^{th}	Thermal characteristic time	s
ϑ_1^1	Temperature change (process complete)	°C
ϑ_R	Temperature change in the rock	°C
$\dot{\vartheta}_o$	Temperature change rate	°C/s
θ_{av}	Average temperature in a fluid column	°C
θ_l	Cavern average temperature	°C
θ_{gr}	Temperature at ground level	°C
θ_{gr}^o	Amplitude of temperature variation at ground level	°C
θ_n	Temperature measured by the n^{th} gauge in the wellhead	°C
θ_R	Rock temperature	°C
θ_R^-	Natural rock temperature	°C
θ_{ref}	Temperature reference for the calculation of saturated brine density and concentration	°C
υ	Parameter for calculation of the heating of a spherical cavern	—
V	Cavern volume	m^3

Symbol	Parameter	Unit
V^o	Initial cavern volume	m^3
V_b	Brine volume in cavern	m^3
V_g	Gas volume in cavern	m^3
V_g^o	Initial nitrogen volume in an NIT	m^3
V_{perm}	Volume fluid lost to permeation	m^3
V_b^o	Starting brine volume	m^3
V_b^f	Ending brine volume	m^3
V_c^f	Ending cavern volume	m^3
V_c^o	Starting cavern volume	m^3
V_h^o	Hydrocarbon volume in cavern	
ϖ	Harmonic wavelength	/s
$v_g\left(v_g^1, v_g^f\right)$	Gas volume injected (starting, ending volumes)	m^3
v_{Inj}, v^{Inj}	Volume brine injected into cavern	m^3
v_{leak}	Volume of leaked hydrocarbon	m^3
v_{salt}	Volume of salt dissolved	m^3
v^{with}	Volume of brine withdrawn (expelled)	m^3
v_o^{with}	Volume of brine withdrawn initially	m^3
v_{leak}^{app}	Apparent volume of leaked hydrocarbon	m^3
W	Function for calculation of the heating of a spherical cavern	—
x	Cavern volume fraction occupied by hydrocarbon	—
z	Depth	m
ξ	Parameter for the calculation of saturated brine concentration	$/°C^2$

15.0 REFERENCES

ATG Manual, 1985. *Gas Transport and Distribution Handbook* (Manuel pour le transport et la distribution du gaz. Titre XIII, Stockages Souterrains de Gaz), Association Technique de l'Industrie du Gaz en France, Paris, 333 pages (in French).

Baar, C. A., 1977. "Applied Salt Rock Mechanics, 1," *In Developments in Geotechnical Engineering* 16-A, 143–147, Elsevier Science, Amsterdam.

Beasley, R. R., 1982. *Strategic Petroleum Reserve (SPR) Oil Storage Cavern Sulphur Mines 2-4-5 Certification Tests and Analysis*, SAND81-2070, Sandia National Laboratories, Albuquerque, NM.

Bérest, P., B. Brouard, and G. Durup, 1995. "Some Comments on the MIT," *Solution Mining Research Fall Meeting*, San Antonio. TX.

Bérest P., J. Bergues, B. Brouard, G. Durup, and B. Guerber, 1996. "A Tentative Evaluation of the MIT," *Solution Mining Research Institute Fall Meeting*, Houston, TX.

Bérest, P., J. Bergues, and B. Brouard, 1999. "Review of Static and Dynamic Compressibility Issues Relating to Deep Underground Caverns, *Int. J. Rock Mech. Min. Sci.*, 36(8), 1031–1049.

Bérest, P., B. Brouard, and J. G. Durup, 2001a. "Tightness Tests in Salt Cavern Wells." *Oil & Gas Science and Technology Journal – Rev. IFP*, Vol. 56, 5, pp. 451–469.

Bérest, P., J. Bergues, B. Brouard, J. G. Durup, and B. Guerber, 2001b. "A Salt Cavern Abandonment Test," *Int. J. Rock Mech. Min. Sci.* 38 (2), pp. 343–355.

Bérest, P., B. Brouard, and G. Durup, 2002. "Tightness Tests in Salt-Cavern Wells," *Solution Mining Research Institute Spring Meeting*, Banff, Canada, pp. 1–26.

Blair, R. W., 1998. "Mechanical Integrity Test (MIT) Nitrogen Interface Method," Solution Mining Research Institute Short Course, *Solution Mining Research Institute Spring Meeting*, 7th Speaker.

Boucly, P., 1981. "In Situ Experience and Mathematical Representation of the Behavior of Rock Salt Used in Storage of Gas," *Proceedings, First Conference on The Mechanical Behavior of Salt*, Pennsylvania State University, University Park, PA, November 9–11, H. R. Hardy, Jr. and M. Langer (eds.), Trans Tech Publications, Clausthal, Germany, 1984, pp. 453-471.

Boucly, Ph. and J. Legreneur, 1980. "Hydrocarbon Storage in Cavities Leached Out of Salt Formations," *Proceedings, International Symposium Rock Store*, M. Bergman (ed.), Pergamon, Vol. I, pp. 251–257.

Brace, W. F., 1980. Permeability of Crystalline and Argillaceous Rocks, *Journal of Rock Mechanics and Mining Science*, 17, pp. 241-251.

Brace, W. F., 1988. "Permeability of Crystalline and Argillaceous Rocks," *International Journal of Rock Mechanics and Mining Science*, 17, pp. 241–251.

Branka, S., M. Mazur, and Z. Jasinski, 2002. "MIT in Gora Underground Cavern Oil and Fuel Storage," *Solution Mining Research Institute Fall Meeting*, Bad Ischl, pp. 65–73.

Brasier, F. M., 1990. "Assuring the Integrity of Solution Mining Operations," *Solution Mining Research Institute Fall Meeting*, Paris, France.

Brouard, B., 1998. *On the Behavior of Solution-Mined Caverns* (in French), Thesis Dissertation, École Polytechnique, France.

Brouard, B. and P. Bérest, 1998. "A Classification of Salt According to Their Creep Properties," *Solution Mining Research Institute Spring Meeting*, New Orleans, LA, pp. 18–38.

Brouard B., P. Bérest, and J. Couteau, 1997. "Influence of the Leaching Phase on the Mechanical Behavior of Salt Caverns," *Solution Mining Research Institute Spring Meeting*, Cracow, Poland, pp. 37–49.

Brouard, B., P. Bérest, and J. G. Durup, 2001. "In-Situ Salt Permeability Testing," *Solution Mining Research Institute Fall Meeting*, Albuquerque, NM, pp. 139–157.

Brouard, B., P. Bérest, J. Y. Héas, D. Fourmaintraux, P. de Laguérie, and T. You, 2004. "An In Situ Creep Test in Advance of Abandoning a Salt Cavern," *Solution Mining Research Institute Fall Meeting*, Berlin, Germany, pp. 45–64.

Carslaw, H. S. and J. C. Jaeger, 1959. *Conduction of Heat in Solids*, Oxford University Press.

CH2M HILL, Inc., 1995. *Technical Manual for External Well Mechanical Integrity Testing Class-III Salt Solution Mining Wells*, report for The Solution Mining Research Institute.

Charpentier, J. P., P. Bérest, and P. A. Blum, 1999. "Creep of a Rock Salt Under Small Loading," *Solution Mining Research Institute Fall Meeting*, Washington, DC, pp. 11–24.

Cole, R., 2002. "The Long Term Effects of High Pressure Natural Gas Storage on Salt Caverns," *Solution Mining Research Institute Spring Meeting*, Banff, Canada, pp. 75–97.

Colin, P. and T. You, 1990. "Salt Mechanics Through 20 Years Experience at the Manosque Facility," *Solution Mining Research Institute Spring Meeting*, Paris, France.

Crotogino, F. R., 1981. "Salt-Cavern In-Situ Testing From the Constructor's and the Operator's Viewpoint," *Proceedings, First Conference on The Mechanical Behavior of Salt*, Pennsylvania State University, University Park, PA, November 9–11, H. R. Hardy, Jr. and M. Langer (eds.), Trans Tech Publications, Clausthal, Germany, 1984, pp. 613–628.

Crotogino, F. R., 1995. *External Well Mechanical Integrity Testing/Performance, Data Evaluation and Assessment*, SMRI Research Report 95-0001-S, prepared for Solution Mining Research Institute.

Crotogino, F. R., 1996. "SMRI References for External Well Mechanical Integrity Testing/Performance, Data Evaluation and Assessment, Summary of the Final Project Report," SMRI 94-0001, *Solution Mining Research Institute Spring Meeting*, Houston, TX [the paper refers to Report 94-0001; in fact the correct reference is likely to be 95-0001-S].

Dale, T. and L. D. Hurtado, 1996. "WIPP Air-Intake Shaft Disturbed Rock Zone Study," *Proceedings, Fourth Conference on The Mechanical Behavior of Salt*, École Polytechnique, Montreal, Canada, June 17–18, M. Aubertin and H. R. Hardy, Jr. (eds.), Trans Tech Publications, Clausthal, Germany, 1998.

DeVries, K. L., 1988. *Viscoplastic Laws for Avery Island Salt*, RSI-0333, prepared by RE/SPEC Inc., Rapid City, SD, for Stone & Webster Engineering Corporation, Boston, MA (quoted by Van Sambeek, 1993).

Diamond, H. W., 1989. "The Water-Brine Interface Method, an Alternative Mechanical Integrity Test for Salt Solution Mining Wells," *Solution Mining Research Institute Fall Meeting*, San Antonio, TX.

Diamond, H. W., B. M. Bertram, P. S. French, G. D. Petrick, M. J. Schumacher, and J. B. Smith, 1993. "Detecting Very Small Casing Leaks Using the Water-Brine Interface Method," *Proceedings, 7th Symposium on Salt*, Kyoto International Conference Hall, April 6–9, 1992, Kyoto, Japan, H. Kakihana; H. R. Hardy, Jr.; T. Hoshi; and K. Toyokura (eds.), Elsevier Science Publishers B.V., Amsterdam, The Netherlands, Vol.1, pp. 363-368.

Denzau, H. and F. Rudolph, 1997. "Field Test for Determining the Convergence of a Gas Storage Cavern Under Load Conditions Frequently Changing Between Maximum and Minimum Pressure and Its Finite Element Modeling," *Solution Mining Research Institute Spring Meeting*, Cracow, Poland, pp. 71–84.

Durup, J. G., 1991. "Relationship Between Subsidence and Cavern Convergence at Tersanne (France)," *Solution Mining Research Institute Spring Meeting*, Atlanta, GA.

Durup, J. G., 1994. "Long Term Tests for Tightness Evaluations With Brine and Gas in Salt," *Solution Mining Research Institute Fall Meeting*, Hannover, Germany.

Edler, D., R. Scheler, and F. Wiesner, 2003. "Real Time Interpretation of Tightness Tests Investigating the Casing Shoe Region of Final Cemented Casings in Gas Storage Cavern Wells," *Solution Mining Research Institute Spring Meeting*, Houston, TX, pp. 251–259.

Ehgartner, B. L. and J. K. Linn, 1994. "Mechanical Behavior of Sealed Solution-Mined Caverns," *Solution Mining Research Institute Fall Meeting*, Houston, TX.

Goin, K. L., 1983. *A Plan for Certification and Related Activities for Department of Energy–SPR Oil Caverns*, SAND83-2005, Sandia National Laboratories, Albuquerque, NM.

Hardy, H. R. Jr., C. R. Chabannes, and M. Mrugola, 1983. "Laboratory and Theoretical Studies Relative to the Design of Salt Caverns for the Storage of Natural Gas," *Proceedings, 6th Symposium on Salt*, B. C. Shreiber and H. L. Harner (eds.), Salt Institute, Vol. I, pp. 385–416.

Heitmann, N. A., 1987. "Experience With Cavern Integrity Testing Using Nitrogen Gas," *Solution Mining Research Institute Spring Meeting*, Tulsa, OK.

Heusermann, S., 1993. "Measurements of Initial Rock Stress at the Asse Salt Mine," *Proceedings, Third Conference on The Mechanical Behavior of Salt*, École Polytechnique, Palaiseau, France, September 14–16, M. Ghoreychi; P. Bérest; H. R. Hardy, Jr.; and M. Langer (eds.), Trans Tech Publications, Clausthal, Germany, 1996, pp. 101–114.

Hugout, B., 1984. "Mechanical Behavior of Salt Cavities–In Situ Tests–Model for Calculating the Cavity Volume Evolution," *Proceedings, Second Conference on The Mechanical Behavior of Salt*, Federal Institute for Geosciences and Natural Resources, Hannover, Federal Republic of Germany, September 24–28, H. R. Hardy, Jr. and M. Langer (eds.), Trans Tech Publications, Clausthal, Germany, 1988, pp. 291-310.

Hunsche, U., 1991. "Volume Change and Energy Dissipation in Rock Salt During Triaxial Failure Tests," *Collection Mechanics of Creep Brittle Materials* 2, A. C. F. Cocks and A. R. S. Ponter (eds.), pp. 172–182.

Jordan, C. W., 1987. "Cased Hole Logging for Determining Mechanical Integrity of Storage Wells," *Solution Mining Research Institute Spring Meeting*, Tulsa, OK.

Kelly, S. L. and J. A. Fleniken, 1999. "The Development of Cement Evaluation Quality Control Measures for Cavern Wells," *Solution Mining Research Institute Spring Meeting*, Las Vegas, NV, pp. 193–225.

Kunstman, A. S. and K. M. Urbanczyk, 1995. "Computer Simulation of Temperature Distribution Around Well and Cavern During Leaching," *Solution Mining Research Institute Spring Meeting*, San Antonio, TX.

Menzel, W. and W. Schreiner, 1983. "Results of Rock Mechanical Investigations for Establishing Storage Cavern in Salt Formations," *Proceedings, 6th Symposium on Salt*, B. C. Shreiber and H. L. Harner (ed.), Salt Institute, Vol. I, pp. 501–510.

Munson, D. E., 1997. "Constitutive Model of the Creep of Rock Salt Applied to Underground Room Closure," *Int. J. Rock Mech. Min. Sc. Geomech. Abst.* 34(2), pp. 233–247.

Munson, D. E., 1998. *Analysis of Multistage and Other Creep Data for Domal Salts*, SAND98-2276, Sandia National Laboratories, Albuquerque, NM.

Munson, D. E., 1999. "Transient Analysis for the Multimechanism-Deformation Parameters of Several Domal Salts," *Solution Mining Research Institute Fall Meeting*, Washington DC, pp. 275–298.

Munson, D. E., A. F. Fossum, and P. E. Senseny, 1989. "Approach to First Principles Model Prediction of Measured WIPP In Situ Closure in Salt," *Proceedings, 30th U.S. Symposium on Rock Mechanics*, West Virginia University, Morgantown, WV, June 19–22, A. W. Khair (ed.), A. A. Balkema, Rotterdam, pp. 673–680 (quoted by Van Sambeek, 1993).

Nelson P. E. and L. L. Van Sambeek, 2003. *State-of-the-Art Review and New Techniques for Mechanical Integrity Tests of (Gas-Filled) Natural Gas Storage Caverns*, 2001-4-SMRI, prepared for Solution Mining Research Institute.

Pouya, A., 1991. "Correlation Between Mechanical Behavior and Petrological Properties of Rock Salt," *Proceedings, 32nd U.S. Symposium on Rock Mechanics*, University of Oklahoma, Norman, OK, July 10–12, J. C. Roegiers (ed.), A. A. Balkema, Rotterdam, pp. 385–392.

Quast, P. and M. W. Schmidt, 1983. "Disposal of Medium- and Low-Level Radioactive Waste (MLW/LLW) in Leached Caverns," *Proceedings, 6th Symposium on Salt*, B. C. Schreiber and H. L. Harner (eds.), The Salt Institute, Vol. II, pp. 217–234.

Quintanihla de Menezes, J. E. and D. Nguyen Minh, 1996. "Long Term Subsidence, Prediction Above Storage Cavity Fields in Salt Layers," *Solution Mining Research Institute Fall Meeting*, Cleveland, OH, pp. 249–273.

Ratigan, J., 1991. "Ground Subsidence at Mont Belvieu, Texas (Panel Discussion–Surface Subsidence)", *Solution Mining Research Institute Spring Meeting*, Atlanta, GA.

Remizov, V. V., A. G. Pozdnyakov, and A. I. Igoshin1, 2000. "Examination of Rock Salt Underground Cavern Testing for Leak-Tightness by Pressure Alteration," *Solution Mining Research Institute Fall Meeting*, San Antonio, TX, pp. 55–64.

Röhr, H. U., 1974. "Mechanical Behavior of a Gas Storage Cavern in Evaporitic Rocks," *Proceedings, 4th Symposium on Salt*, A.H. Coogan (ed.), Salt Institute, Vol. II, pp. 93–100.

Rokahr R. B., R. Hauck, K. Staudtmeister, and D. Zander-Schiebenhöfer, 2000. "The Results of the Pressure Build-Up Test in the Brine Filled Cavern Etzel K102," *Solution Mining Research Institute Fall Meeting*, San Antonio, TX, pp. 89–103.

Rummel F., K. Benke, and H. Denzau, 1996. "Hydraulic Fracturing Stress Measurements in the Krummhörn Gas Storage Field, Northwestern Germany," *Solution Mining Research Institute Spring Meeting*, Houston, TX.

Senseny, P. E., 1984. "Creep Properties of Four Rock Salts," *Proceedings, Second Conference on The Mechanical Behavior of Salt*, Federal Institute for Geosciences and Natural Resources, Hannover, Federal Republic of Germany, September 24–28, H. R. Hardy, Jr. and M. Langer (eds.), Trans Tech Publications, Clausthal, Germany, 1988, pp. 103–128.

Solution Mining Research Institute, 1998. "Mechanical Integrity Testing of Brine Production and Storage Wells," Technical Class, *Solution Mining Research Institute Spring Meeting*, New Orleans, LA.

Staupendahl, G. and M. W. Schmidt, 1984. "Field Investigations in the Long-Term Deformational Behavior of a 10,000 m^3 Cavity at the Asse Salt Mine," *Proceedings, Second Conference on The Mechanical Behavior of Salt*, Federal Institute for Geosciences and Natural Resources, Hannover, Federal Republic of Germany, September 24–28, H. R. Hardy, Jr. and M. Langer (eds.), Trans Tech Publications, Clausthal, Germany, 1988, pp. 511–526.

Thiel, W. R, 1990. "Alternative Methods for Testing the Integrity of Underground Storage Caverns," *Solution Mining Research Institute Spring Meeting*, Austin, TX.

Thiel, W. R., 1993. "Precision Methods for Testing the Integrity of Solution Mined Underground Storage Caverns," *7th Symposium on Salt*, Kyoto International Conference Hall, April 6–9, 1992, Kyoto, Japan, H. Kakihana; H. R. Hardy, Jr.; T. Hoshi; and K. Toyokura (eds.), Elsevier Science Publishers B.V., Amsterdam, The Netherlands, Vol. I, pp. 377–383.

Thiel, W. R. and J. M. Russel, 2004. "Pressure Observation Testing Solution Mined Underground Storage Caverns in Kansas," *Solution Mining Research Institute Spring Meeting*, Wichita, KS, pp. 186–198.

Thoms, R. L. and G. Kiddoo, 1998. "Well Design for Operations in Salt Formations. Guidelines for Safety Assessment of Salt Caverns," *Proceedings, Technical Class, Solution Mining Research Institute Fall Meeting*, Roma, pp. 113–140.

Van Fossan, N. E., 1983. "The Characterization of Mechanical Integrity for Cased Boreholes Entering Solution Caverns," *Proceedings, 6th International Symposium on Salt*, The Salt Institute, Vol. II, pp. 111–120.

Van Fossan, N. E. and F. V. Whelply, 1985. "Nitrogen as a Testing Medium for Proving the Mechanical Integrity of Wells," *Solution Mining Research Institute Fall Meeting*, Houston, TX.

Van Sambeek, L. L., 1990. "A Simple Method for Modeling the Pressure Build Up or Flow of an Abandoned Solution Well," *Solution Mining Research Institute Spring Meeting*, Austin, TX.

Van Sambeek, L. L., 1993. "Evaluating Cavern Tests and Surface Subsidence Using Simple Numerical Models," *7th Symposium on Salt*, Kyoto International Conference Hall, April 6–9, 1992, Kyoto, Japan, H. Kakihana; H. R. Hardy, Jr.; T. Hoshi; and K. Toyokura (eds.), Elsevier Science Publishers B.V., Amsterdam, The Netherlands, Vol. I, pp. 433–439.

You T., C. Maisons, and M. Valette, 1994. "Experimental Procedures for the Closure of the Brine Production Caverns of the 'Saline de Vauvert' Site," *Solution Mining Research Institute Fall Meeting*, Hannover, Germany.

Vrakas, J., 1988. "Cavern Integrity Testing on the SPR Program," *Solution Mining Research Institute Spring Meeting*, Mobile, AL.

Project: Gas Oil Storage Twente (Clovis)

Mechanical Integrity Test (MIT)

at AkzoNobel Cavern Series 472

for

AkzoNobel Industrial Chemicals B.V.
Boortorenweg 27
P.O. Box 25
7550 GC, Hengelo, The Netherlands

KBB UT Project No.:	5305-881095		
Author(s):			
	Checked: NH	Approved:	NH
Date:	16 January 2015	Revision:	01

KBB Underground Technologies GmbH • [illegible] • [illegible]
Tel. +49 (0) 51 [illegible] • Fax +49 (0) [illegible]
E-Mail: info@kbbut.de • Website: www.kbbut.de

DEEP. Underground Engineering GmbH • Eschhauser Allee 30 • D-26160 Bad Zwischenahn
Tel. +49 (0)4403 9322-0 • Fax +49 (0)4403 9322-11
E-Mail: info@deep.de • Website: www.deep.de

Table of Contents

1 Introduction

AkzoNobel Industrial Chemicals B.V. (AkzoNobel) is investigating the usage of the brine caverns 472 and 381 for oil product storage. The caverns 472 and 381 have each three access boreholes. Before converting the brine caverns to oil storage, all cavern boreholes have to be tested for hydraulic tightness by a mechanical integrity test (MIT).

The MIT, which is part of the cavern acceptance procedure, is performed to check the suitability of the area around the last cemented casing shoe (LCCS), i.e. the bond between the last cemented casing, cement and salt, for the intended oil storage.

In 2013, the general pressure integrities of the caverns 472 and 381 were checked by hydraulic pressure tests. Thereby, brine was injected in each cavern to increase the cavern pressure to a level, which is required for MIT performance respectively for planned oil storage. During the hydraulic pressure tests at 472 and 381, it was found that the cavern floor, which is formed by the Solling Formation, is not entirely impermeable.

On this basis, the MIT at the cavern wells of 472 and 381 were planned as interface tests. For MIT performance, the test medium oil was injected in the wells. In each well, the oil/brine interface level was adjusted below the LCCS in the cavern neck area creating an independent and separated test volume for individual test evaluation per well, The MIT used test pressures at the LCCS above the range of the later maximum permissible storage pressure.

During performance of the first MIT at cavern series 472 in October/November 2014, it was realised, that the oil/brine interface levels at all wells were positioned in cemented cavern neck regions. Therewith, it was not possible to check the potential flow path between cement and salt. Therefore, after performing cavern neck caliper and sonar surveys, the MIT at cavern series 472 was repeated in November/December 2014 with oil/brine interface levels adjusted in uncemented cavern neck areas. By this MIT, described in the document as "second MIT", all critical leak paths in the area of the LCCS – namely between steel and cement, between cement and salt and the rock salt below the cement – were hydraulic tightness tested.

The subject of this document is the procedure, the results and the evaluation of the second MIT at the three cavern wells 472, 473 and 474 of AkzoNobel cavern series 472.

2 Basic Well and Pressure Data

The basic well data of cavern 472 are included in Table 1.

The setup of the second MIT at cavern 472 is displayed in Enclosure 1. The MIT at the cavern wells 472, 473 and 474 were each performed on the 7" last cemented casing having installed a 4 ½" tubing. At the outsides of each 4 ½" tubing, SOCON Blanket Control Systems (BCS) were installed. The BCS was used to measure the oil/brine interface level depth in the oil filled test volume in the 4 ½" x 7" annulus respectively in the annulus between 4 ½" and cavern neck.

Table 1: Depths and diameters of wells 472, 473 and 474 for 2nd MIT

	Well 472	Well 473	Well 474
Depth LCCS (7", 23 lbs/ft) in m MD	444.4	443.2	444.2
ID LCCS (7", 23 lbs/ft) in mm	161.4	161.4	161.4
OD 4 ½" tubing in mm	114.3	114.3	114.3
Depth BCS sensor 1 in m MD	446.6	445.2	446.4
Depth BCS sensor 20 in m MD	448.5	447.1	448.3
Offset (MD-TVD) in m	0.0	0.0	0.0
Cavern volume 472 in m³	approx. 160,000		

The pressures and pressure gradients during oil operation, advised by the rock mechanical expert IfG, Leipzig, compared to the maximum observed values during MIT are summarised in Table 2 (for detailed test pressure calculation, see Chapter 3.3). Please note, that the minimum observed MIT pressure at the LCCS had always been at least 1.2 bar above the minimum test pressure desired by the rock mechanical expert.

Table 2: Pressure gradients and pressures for 2nd MIT at wells 472, 473 and 474

	Well 472	Well 473	Well 474
Max. permissible pressure gradient during oil operation in bar/m	0.150 bar/m + additional 5 bar = 0.161 bar/m	0.150 bar/m + additional 5 bar = 0.161 bar/m	0.150 bar/m + additional 5 bar = 0.161 bar/m
Max. permissible pressure at LCCS during oil operation = min. desired MIT pressure at LCCS in bar	**71.7**	**71.5**	**71.6**
Min. observed MIT pressure gradient in bar/m	0.164	0.164	0.164
Min. observed MIT pressure at LCCS in bar	**72.9**	**72.8**	**73.0**
Max. observed MIT pressure gradient in bar/m	0.165	0.165	0.165
Max. observed MIT pressure at LCCS in bar	73.4	73.3	73.5

3 General MIT Programme

The second MIT was prepared and performed according to the specification and work programme prepared by DEEP./KBB UT and AkzoNobel[1].

3.1 Test Procedure

In general, the sequence of work steps for the second MIT was as follows:

- Cavern neck survey at all wells
- Run in hole of a 4 ½" tubing including BCS at all wells, installation of well heads
- Diesel oil injection in 4 ½" x 7" annulus at all wells and oil/brine interface level adjustment at all wells
- Installation of well head pressure recording system at 4 ½" and 4 ½" x 7" annulus at all wells, recording of ambient temperatures at all well heads
- Brine injection in 4 ½" of well 474 for test pressure adjustment
- Damping period for 4 days including brine injection for test pressure readjustment
- MIT performance for 5 days with observation of oil/brine interface level depths by BCS in 24 hour-intervals, resulting in one reference measurement and 4 interval measurements, i.e. 4 test intervals, optional brine injection for test pressure readjustment
- MIT evaluation
- Release oil at all wells, release brine at 4 ½" of well 474
- Uninstallation of well head and pull out of hole of the 4 ½" tubing at all wells

At all wells, the overall technical hydraulic tightness of the following sections was confirmed (see also Enclosure 1 for MIT setup):

- Test well head
- 4 ½" tubing in the range between well head to oil/brine interface level
- 7" LCCS
- Steel/cement bond in the area of the 7" LCCS

[1] DEEP. Underground Engineering GmbH, KBB Underground Technologies GmbH, AkzoNobel Industrial Chemicals B.V.:" Project: Gas Oil Storage Twente (Clovis) – Specification Mechanical Integrity Test (MIT)", 09 October 2014.

- Cemented cavern neck in the range between 7" LCCS and lower end of cement in cemented cavern neck
- Cement/salt bond at the lower end of cement in the cemented cavern neck
- Rock salt of the cavern neck in the range between lower end of cement and the oil/brine interface level

3.2 Test Criterion

The following test criterion was agreed during MIT planning: The criterion is determined by the accuracy of the MIT evaluation.

The evaluation, which is presented in detail in Chapter 5.1, is performed by geometrical oil volume balancing during testing time. Then, it is possible to calculate a leak rate for each of the 4 test intervals and an average leak rate for the overall testing time.

Regarding the test criterion: If the calculated average apparent leak rate stays within the boundaries of the overall MIT accuracy, the LCCS of a well is to be defined as "technically hydraulic tight".

Extraordinary circumstances require a detailed examination, e.g. an inflow of former blanket oil in the test volume, or e.g. when a BCS step change is observed directly after MIT start it may be possible, that the oil/brine level has been adjusted directly below a BCS sensor.

3.3 Test Pressure Calculation

The test pressures at the LCCS were calculated on the basis of the maximum permissible pressure gradient during oil operation advised by the rock mechanical expert IfG, Leipzig (see Table 3). The recommended pressure gradient was 0.15 bar/m plus an additional pressure range of 5 bar. Therefore, the maximum permissible pressures during oil operation at the LCCS, which represented the minimum test pressures at the LCCS, were computed according to Equation 1:

$$p_{LCCS\,oil} = grad\,p_{oil} * d_{LCCS} + 5\ bar \qquad (1)$$

with:

$p_{LCCS\,oil}$	[bar]	Maximum permissible pressure at LCCS during oil operation
grad p_{oil}	[bar/m]	Recommended pressure gradient by IfG, Leipzig, during oil operation
d_{LCCS}	[m TVD=m MD]	Depth of 7" LCCS

Based on the maximum permissible pressures during oil operation respectively the minimum test pressures at the LCCS, the minimum MIT well head pressures at 4 ½" (brine side) and 4 ½" x 7" (oil side) were derived by using Equation 2 under consideration of the corresponding specific weights:

$$p_{wh} = p_{LCCS\,oil} - \gamma * g * d_{LCCS} * 10^{-5} \quad (2)$$

with:

p_{wh}	[bar]	Minimum MIT well head pressure
γ	[kg/m³]	Specific weight (brine: 1,200 kg/m³, Diesel oil: 830 kg/m³)
g	[m/s²]	Gravitational acceleration

Table 3: Pressure calculations for 2nd MIT at wells 472, 473 and 474

	Well 472	**Well 473**	**Well 474**
Depth LCCS (7", 23 lbs/ft) in m TVD	444.4	443.2	444.2
Max. permissible pressure at LCCS during oil operation = min. MIT pressure at LCCS in bar	71.7	71.5	71.6
Min. MIT well head pressure at 4 ½" (brine side) in bar	19.4	19.4	19.4
Min. MIT well head pressure at 4 ½" x 7" (oil side) in bar	35.5	35.4	35.5

Due to the not entirely impermeable cavern floor (Solling Formation), it was planned to readjust the test pressures during the MIT by optional brine pumping. For MIT performance, all pressures should not fall below the minimum MIT pressures at any time. Therefore, it was planned to exceed the minimum MIT well head pressures, mentioned in Table 3, by 1 to 2 bar. This means, that during the whole testing period the wells were tested at higher pressures than they will ever experience during oil operation.

4 MIT Performance

4.1 Test Preparation

4.1.1 Cavern Neck Survey

On 14/11/2014 at wells 472 and 474, cavern neck caliper surveys were performed[2] [3]. Each run was executed with a 4 arm caliper (Tool no.: SOCON Kaliber 4 Arm 575/1) in a depth range starting from cavern roof and ending above the LCCS. The results of the caliper runs are displayed in Figure 1 and Figure 2. In these figures, the lower ends of cement in the cavern necks can easily be seen. For well 472, the lower end of cement is 446.6 m MD, for well 474, the depth is 446.4 m MD. Below these depths, there are uncemented salt necks.

Figure 1: Evaluation SOCON caliper run at well 472

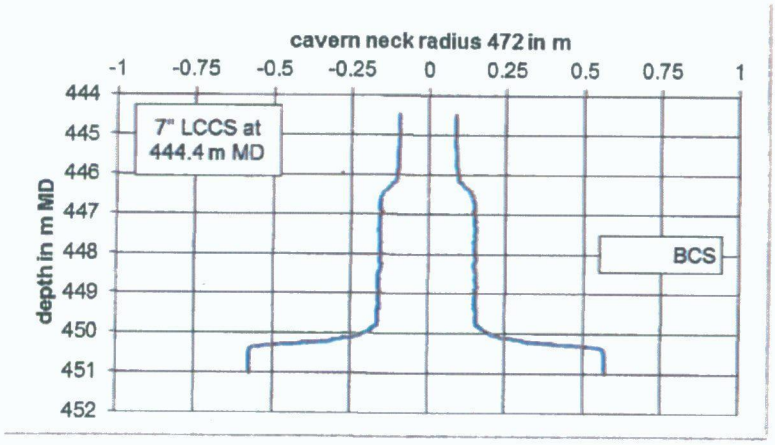

Figure 2: Evaluation SOCON caliper run at well 474

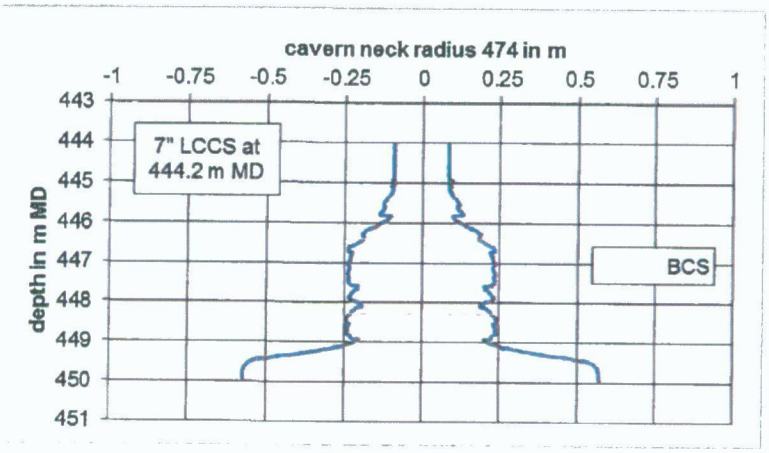

[2] SOCON GmbH: Caliper Log Well 472 "472_069_0005_L03_20141114.asc", 14 November 2014.
[3] SOCON GmbH: Caliper Log Well 474 „474_101_0004_L02_20141114.asc", 14 November 2014.

On 17/11/2014 at well 473, a cavern neck sonar survey was performed (Tool no.: SOCON Echo tool BSF2 72)[4]. The survey was run in the depth range from cavern roof to 20 cm below the LCCS. The evaluation of the sonar survey can be seen in Figure 3. Below the LCCS of 473, a larger bulb is visible. Below this bulb at 445.2 m MD, there is an uncemented salt cavern neck.

Figure 3: Evaluation SOCON sonar survey at well 473

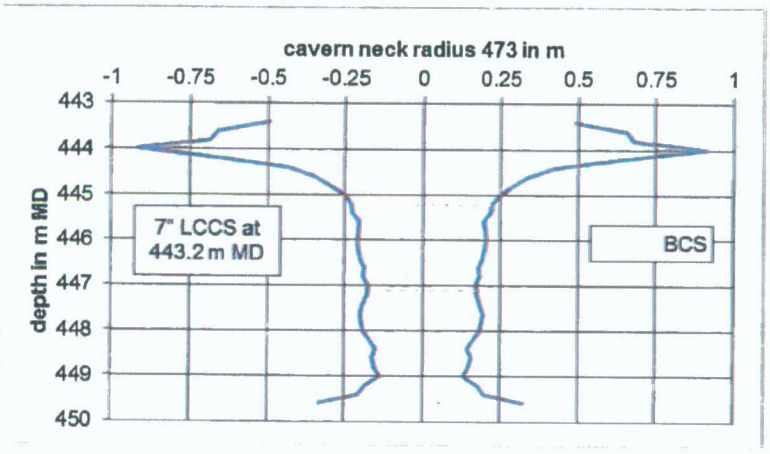

The volume lists of well 472, 473 and 474 can be found in Enclosure 2 to 4.

4.1.2 Blanket Control System

Subsequent to the neck surveys, the 4 ½" tubings with the SOCON Blanket Control System (BCS) for oil/brine interface level monitoring were run in hole respectively set in positions (see Enclosure 1 for MIT setup).

The BCS consisted of 20 sensor elements. These elements were fixed on the outsides of the 4 ½" tubings. The distance between the sensor elements was 10 cm, which also represents the measuring accuracy of the interface detection. The downhole BCS communicated via data cable with an aboveground data interface device (see Figure 4). The interface level depth detection by the BCS sensors was performed by conductivity measurement. The intense change in conductivity gave the position of the interface.

This means for the conductivity profile example in Figure 4: the sensor element no. 11 is covered in oil, sensor no. 12 is in brine. Therewith, the interface is located at a position between sensor no. 11 and 12. The interface depth of 445.40 m, which is shown in the display, corresponds to the depth of sensor no. 12. So in fact, the interface is somewhere between 445.40 and 445.30 m in this example. As the conductivity at sensor no. 11 is extremely low, it can be concluded, that the level is not very close to sensor no. 11. Furthermore, the temperature at the interface of e.g. 22.1 °C can be monitored.

[4] SOCON GmbH:"Echo Log Hengelo B 473 Shaft Survey", Doc.no. 144 102, 17 November 2014.

Figure 4: SOCON BCS aboveground data interface display

At cavern series 472, the BCS at each well were hang off at depths, that had been identified as uncemented salt neck sections by the neck surveys (see Chapter 4.1.1). The setting depths of the BCS are also visible in the cavern neck cross sections in Figure 1 to Figure 3. In Enclosure 5 to 7, the detailed cavern neck cross sections including corresponding BCS sensor numbers are included (based on caliper and sonar surveys).

4.1.3 Well Head Pressure Recording System

On 02/12/2014, KBB UT digital well head pressure and temperature recording systems (Type: UNION ESSIII STATION) were assembled at all well heads (see Enclosure 1 for MIT setup).

At the 4 ½" tubing and at the 4 ½" x 7" annulus, digital pressure sensors with a measuring error of 0.09 % regarding the maximum measuring range were installed. The maximum pressure range of all pressure sensors was 150 bar. The sample rate of the pressure sensors was set to 1 s, i.e. the pressure situation was checked every second. When a pressure change of 0.003 % of the maximum pressure range was observed, the changed well head pressure value was recorded. The ambient temperatures were measured near the well heads for optional correlation with the well head pressures. The serial numbers of the KBB sensors are summarised in Table 4.

Table 4: KBB UT sensor serial numbers of UNION ESSIII STATIONs

	Well 472	Well 473	Well 474
Pressure at 4 ½"	AAE 2188 E	AAE 1774 D	AAE 4058 G
Pressure at 4 ½" x 7"	AAE 2187 E	AAE 1755 D	AAE 4059 G
Ambient Temperature	AAH 0105 E	AAH 0095 D	AAH 0208 G

During the actual MIT a second well head pressure recording system of GEOSTOCK was installed as well. This higher accuracy system moved along the three wells and was installed at each well for 1 to 1.5 day. It will be used in the Peer Review on the MIT, which will be undertaken by GEOSTOCK. Data, results and conclusions will be reported in the Peer Review report by GEOSTOCK.

4.1.4 Oil Injection

On 02/12/2014, Diesel oil was injected in all wells using an AkzoNobel oil pumping truck according to the following procedure:

As a first step, oil was pumped until one of the first BCS sensor elements was covered in oil. After that, more oil was injected until more or less the complete BCS was in oil. The pumped oil volumes were measured by an AkzoNobel oil flow meter. After a damping period overnight, oil was BCS stepwise released by measuring the backflowing oil volumes on 03/12/2014. After that, oil was pumped in the well again and the oil/brine interface was adjusted for MIT performance. By this procedure, possible pockets in the cavern neck walls were filled with oil. Furthermore, the pumped and released oil volumes could be compared to the expected values according to the volume lists in Enclosure 2 to Enclosure 4.

Especially at well 473, the oil volume per BCS step during pump and release was found a little larger than expected. However, the comparison of pumped/released and expected oil volumes showed a very good correspondence. Due to this and because of the consistent cavern neck cross section of well 472, the release and pump-in cycle at well 472 was not carried out.

The oil pump and release records, which were only used for consistency checks regarding the cavern neck surveys, are to be found in Enclosure 8. The MIT evaluations were exclusively based on the cavern neck survey data.

4.1.5 Brine Injection

On 03/12/2014, brine injection was started at 4 ½" of well 474 for test pressure adjustment. Therefore, a tank, a brine pump, HP lines, a check valve, a gate valve and a brine flow meter were rigged up. The brine flow meter was a portable ultrasonic clamp-on metering device Krohne Optisonic 6300 P, supported by ICM, Hamburg. At first, brine was injected to a well head pressure of 31.1 bar at 4 ½" x 7" of well 474 (100 m³ brine pumped). The well head pressure data including pumped brine volumes are attached in Enclosure 9. On 04/12/2014, brine was pumped to the test pressure of 37.5 bar at 4 ½" x 7" of well 474 (in total 187.5 m³ brine pumped). On 05/12/2014 and on 07/12/2014, brine injections for pressure readjustment were performed. Thereby, the observed pressure decreases per day reduced from 1.1 bar/24 h to 0.5 bar/24 h. This reduction may

be due to ongoing saturation of the slightly permeable Solling Formation. The pumped brine volumes decreased from 12.5 m³ on 05/12/2014 (in total 200 m³) to 9 m³ on 07/12/2014 (in total 209 m³).

4.2 MIT Execution

On 08/12/2014, the actual MIT at cavern series 472 was started. The MIT was performed for 5 days with observation of the oil/brine interface level depths by BCS in 24 hour-intervals, resulting in one reference measurement and 4 interval measurements. Therewith, 4 test intervals for oil volume balancing respectively leak rate calculation were available. The daily measurements were carried out at 13:00. The MIT was finalised on 12/12/2014 at 13:00. The observed well head data and the interface depth data can be found in Enclosures 10 to 11. The detailed interface depth data including conductivity values and temperatures near the interface are also included in the daily reports in Enclosure 12. It should be noticed, that a shown interface depth of e.g. 447.5 m MD in fact corresponded to an interface between 447.4 m MD and 447.5 m MD.

On 08/12/2014 after performing the reference measurement, the only brine injection during testing time for test pressure readjustment was executed. The observed pressure decrease from 07/12/2014 to 08/12/2014 was again 0.5 bar/24 h. Nevertheless, the well head pressures during testing time never came below the minimum required test well head pressures of Table 3. The pumped brine volume on 08/12/2014 was 3.8 m³ (in total 212.8 m³). After that, the test pressures stayed above the minimum MIT pressures for the remaining testing time including a sufficient pressure reserve. No further brine injection was required. On the last MIT day on 12/12/2014 13:00, the well head pressure at 4 ½" x 7" of well 474 was still 36.9 bar with a minimum test pressure (respectively maximum permissible pressure during oil operation) at 4 ½" x 7" at well 474 of 35.5 bar.

After ending the MIT on 12/12/2014, pressures were released from the cavern as well as the testing medium oil. After that, the 4 ½" tubings at all wells were pulled out of hole.

5 MIT Evaluation

5.1 Theoretical Basics

The MIT evaluation was performed by geometrical oil volume balancing over testing time. The influences of temperature changes in the oil test volumes and the compressibility of oil were not included in test evaluation. The temperature and pressure differences observed at the MIT measurements were relatively low. In this way, the impacts on oil volume changes caused by temperature and pressure effects were also relatively low and could be neglected in the evaluation (see Chapter 5.3 for evaluation data). Only during brine pumping on 07/12/2014 and on 08/12/2014, the cooling effect of the cold brine in the 4 ½" on the warmer oil in the 4 ½" x 7" annulus of well 474 caused a raise of the oil/brine interface level.

During MIT, the enclosed oil volume was calculated using the following Equation 3. The oil volume was dependent on the pipe dimensions of the 7" LCC and on the cavern neck geometry resulting from the cavern neck survey taking the 4 ½" tubing into account:

$$V_{oil} = \frac{\pi}{4} * ID_{LCC}^2 * d_{LCCS} + \sum_{n=1}^{N} \frac{\pi}{4} * \left[ID_{Neck\,n+1}^2 - OD_{Tub}^2\right) * (d_{n+1} - d_n)$$

$$with\ d_1 = d_{LCCS}\ and\ d_N = d_{interface} \qquad (3)$$

with

V_{oil}	[m³]	Enclosed oil volume
ID_{LCC}	[m]	Inner diameter of 7" last cemented casing
ID_{Neck}	[m]	Inner diameter of cavern neck dependent on BCS depth step of volume list
OD_{Tub}	[m]	Outer diameter of 4 ½" tubing
d_n	[m TVD=m MD]	Depth of cavern neck survey step and BCS step according to volume list
$d_{Interface}$	[m TVD=m MD]	Depth of oil/brine interface level

With these data, the oil volumes were determined for the reference measurement and for the 4 interval measurements. With the changes of the oil volume within a test interval, apparent leak rates for 4 test intervals in litre per day in-situ, i.e. under pressure and temperature conditions at the LCCS, were calculated (see Equation 4). For the overall testing time, an average apparent leak rate was computed:

$$LR = \frac{V_{oil}}{t} \qquad (4)$$

with

LR	[l/d in-situ]	Apparent leak rate / average apparent leak rate
t	[d]	Time of interval / overall testing time

5.2 Test Accuracy

Based on the accuracy for oil/brine interface depth detection and based on the accuracy for the cavern neck survey, the MIT overall accuracy was calculated.

This calculation differs from the measurement error equation mentioned in the specification of the MIT[5]. Due to the partially irregular cavern neck geometries, the error equation of the specification was not applicable.

The accuracy of the interface depth detection was determined by the BCS sensor element distance of 10 cm. As a result of this BCS sensor setup, the oil interface level was adjusted during oil injection at a random position between two BCS sensors. The exact position was not known. Therefore, the oil volume, which was present between the starting BCS step at the zero measurement and the overlying BCS step according to the cavern neck survey results excluding the 4 ½" volume, defined the MIT accuracy.

The second parameter, which had direct influence on MIT accuracy, was the cavern neck radius itself measured during the cavern neck survey. For MIT accuracy calculation, the radius of the starting BCS step was increased by an uncertainty factor of 10 %. This factor was applied for the results of the 4 arm caliper survey and also for the results of the sonar survey.

Therewith, the MIT overall accuracy was calculated according to Equation 5 and Table 5 applied to the overall testing time:

$$ACC = \frac{\pi * (acc_{radius} * r_{BCS})^2 * acc_{BCS} - \frac{\pi}{4} * OD_{Tub}^2 * acc_{BCS}}{t} \quad (5)$$

$$= \frac{\pi * (1.1 * r_{BCS})^2 * 0.1 - \frac{\pi}{4} * OD_{Tub}^2 * 0.1}{t}$$

with

ACC	[l/d in-situ]	MIT overall accuracy

[5] DEEP. Underground Engineering GmbH, KBB Underground Technologies GmbH, AkzoNobel Industrial Chemicals B.V.:" Project: Gas Oil Storage Twente (Clovis) – Specification Mechanical Integrity Test (MIT)", 09 October 2014.

acc_{radius}	[-]	Factor for error of radius determination during cavern neck survey
r_{BCS}	[m]	Cavern neck radius in depth of starting BCS step at zero measurement
acc_{BCS}	[m]	Distance between BCS sensor elements
t	[d]	Overall testing time

Table 5: 2nd MIT accuracy parameter

Accuracy for interface level detection in m	0.1
Error for radius of cavern neck survey in %	10.0
Overall testing time in d	4.0

5.2.1 Accuracy at Well 472

For well 472, the MIT accuracy was calculated in the following Table 6. The accuracy was computed according to the accuracy equation 5, the accuracy parameters of Table 5 and according to the cavern neck radius of the starting BCS step listed in the volume list in Enclosure 2.

Table 6: 2nd MIT accuracy for well 472

Interface depth of zero measurement in m MD	Starting BCS step no. of zero measurement	Cavern neck radius of starting BCS step in m	MIT accuracy ACC in l/d in-situ
448.0	15	0.153	+/- 2.0

5.2.2 Accuracy at Well 473

For well 473, the MIT accuracy was calculated in the following Table 7. The accuracy was computed according to the accuracy equation 5, the accuracy parameters of Table 5 and according to the cavern neck radius of the starting BCS step listed in the volume list in Enclosure 3.

Table 7: 2nd MIT accuracy for well 473

Interface depth of zero measurement in m MD	Starting BCS step no. of zero measurement	Cavern neck radius of starting BCS step in m	MIT accuracy ACC in l/d in-situ
446.9	18	0.186	+/- 3.0

5.2.3 Accuracy at Well 474

For well 474, the MIT accuracy was calculated in the following Table 8. The accuracy was computed according to the accuracy equation 5, the accuracy parameters of Table 5 and according to the cavern neck radius of the starting BCS step listed in the volume list in Enclosure 4.

Table 8: 2nd MIT accuracy for well 474

Interface depth of zero measurement in m MD	Starting BCS step no. of zero measurement	Cavern neck radius of starting BCS step in m	MIT accuracy ACC in l/d in-situ
447.5	12	0.237	+/- 5.1

5.2.4 Comparison of Test Accuracies with International Criteria

As already discussed in Chapter 3.2, the above calculated test accuracies were used for test criteria. In order to classify these results, the computed accuracies of the MIT at wells 472, 473 and 474 were compared to a selection of international leak criteria, which can be found in literature (see Table 9).

Table 9: Comparison of test criteria

Reference		Criterion in l/d in-situ
2nd MIT at well 472	Test accuracy = test criterion	+/- 2.0 l/d
2nd MIT at well 473	Test accuracy = test criterion	+/- 3.0 l/d
2nd MIT at well 474	Test accuracy = test criterion	+/- 5.1 l/d
Strategic Petroleum Reserve of the US Department of Energy[6]	Admissible leak rate	+/- 44.0 l/d
Meinecke, Walter, Kruck (2013)[7]	Test accuracy = test criterion	+/- 25.8 l/d
Remizov, Pozdnyakov, Igoshin (2000)[8]	Admissible leak rate	Smaller than 20.0 – 27.0 l/d

[6] Crotogino, F.: „SMRI Reference for External Well Mechanical Integrity Testing/Performance, Data Evaluation and Assessment", SMRI Research Project Report No. 95-0001-S, 1995.
[7] Meinecke, I., Walter, M., Kruck, O.: „A Hydraulic Mechanical Integrity Test of an Oil Cavern using the SoMIT Method", SMRI Fall Technical Conference, Avignon, France, 2013.
[8] Remizov, V. V., Pozdnyakov, A. G., Igoshin, A. I.: „Examination of Rock Salt Underground Cavern Testing for Leak-Tightness by Pressure Alteration", SMRI Fall Meeting, San Antonio, Texas, USA, 2000.

In short, the applied test criteria for the 2nd MIT at AkzoNobel cavern series 472 are in the lower range of admissible leak rates values. This means, the MIT at cavern series 472 were sufficiently exact and allowed a qualified statement regarding technical hydraulic tightness.

5.3 Test Results

In this chapter, the MIT results are presented on a well-by-well basis.

5.3.1 Results at Well 472

The essential test results for well 472 are listed in Table 10. In general, negative leak rates signify an inflow of oil, whereas positive leak rate indicate a loss of oil.

Table 10: 2nd MIT results at well 472

Measurement no.	Time in dd/mm/yy hh:mm	BCS interface level depth in m MD	Calculated oil volume in l	Leak rate LR of intervals in l/d in-situ
Reference	08/12/2014 13:00	448.0	4,671.8	-
First	09/12/2014 13:00	448.0	4,671.8	0.0
Second	10/12/2014 13:00	448.0	4,671.8	0.0
Third	11/12/2014 13:00	447.9	4,665.4	6.4
Fourth	12/12/2014 13:00	447.9	4,665.4	0.0

During testing time, a constant oil/brine interface level depth of 448.0 m MD was observed from the reference until the second measurement (see also Enclosure 11). On the third measurement, the interface level increased by one BCS step to a depth of 447.9 m MD. Then for the fourth measurement, the interface level depth remained constant at 447.9 m MD.

Therefore, the apparent leak rates of all intervals were calculated to 0.0 l/d in-situ, apart from the leak rate of the third test interval, which was computed to 6.4 l/d in-situ. This corresponded to an average apparent leak rate for the overall testing time of 1.6 l/d in-situ. The MIT accuracy for well 472 was calculated to +/- 2.0 l/d in-situ, which represented the test criterion (see Table 6). Therewith, the average leak rate stayed within the boundaries of the determined test criterion. The visualisation of the apparent leak rates and of the MIT accuracy is given in Figure 5.

Figure 5: Apparent leak rates of 2nd MIT at well 472

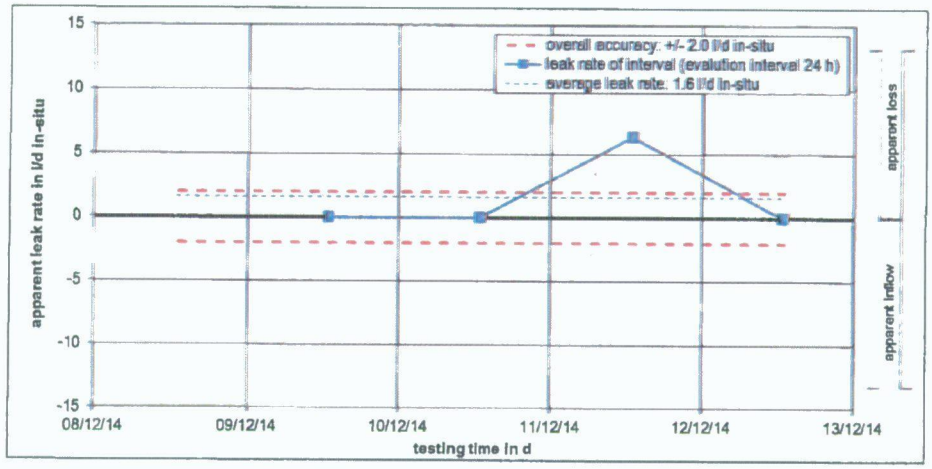

Furthermore, the observed well head pressures during testing time at well 472 were not less than the minimum MIT well head pressures at 4 ½" and 4 ½" x 7" of 19.4 bar and 35.5 bar (see Table 3). The detailed evaluation data including pressure and temperature data is attached in Enclosure 13.

5.3.2 Results at Well 473

The essential test results for well 473 are listed in Table 11. In general, negative leak rates signify an inflow of oil, whereas positive leak rate indicate a loss of oil.

Table 11: 2nd MIT results at well 473

Measurement no.	Time in dd/mm/yy hh:mm	BCS interface level depth in m MD	Calculated oil volume in l	Apparent leak rate of intervals in l/d in-situ
Reference	08/12/2014 13:00	446.9	6,526.9	-
First	09/12/2014 13:00	446.9	6,526.9	0.0
Second	10/12/2014 13:00	446.9	6,526.9	0.0
Third	11/12/2014 13:00	446.9	6,526.9	0.0
Fourth	12/12/2014 13:00	446.8	6,517.1	9.9

During testing time, a constant oil/brine interface level depth of 446.9 m MD was observed from the reference until the third measurement (see also Enclosure 11). Then for the fourth measurement, the interface level depth increased by one BCS step to a depth of 446.8 m MD.

Therefore, the apparent leak rates of all intervals were calculated to 0.0 l/d in-situ, apart from the leak rate of the fourth test interval, which was computed to 9.9 l/d in-situ. This

corresponded to an average apparent leak rate for the overall testing time of 2.5 l/d in-situ. The MIT accuracy for well 473 was calculated to +/- 3.0 l/d in-situ, which represented the test criterion (see Table 7). Therewith, the average leak rate stayed within the boundaries of the determined test criterion. The visualisation of the apparent leak rates and of the MIT accuracy is given in Figure 6.

Figure 6: Apparent leak rates of 2nd MIT at well 473

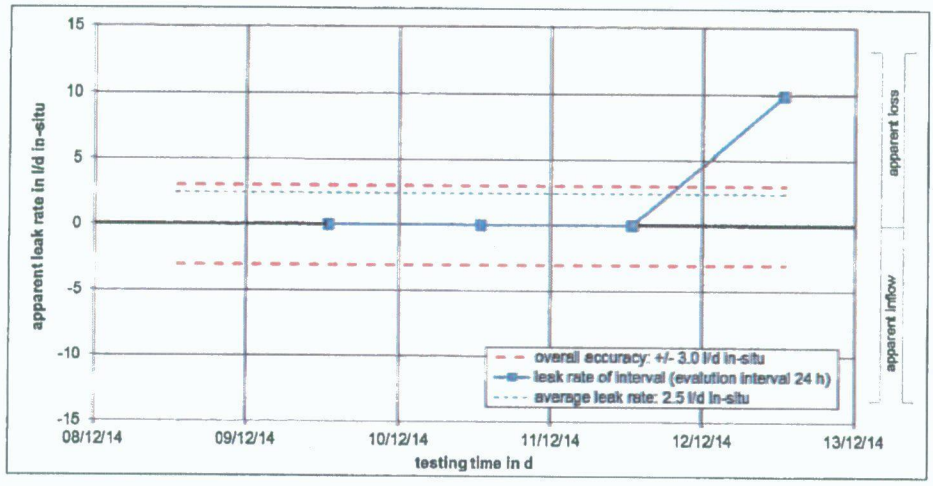

Furthermore, the observed well head pressures during testing time at well 473 were not less than the minimum MIT well head pressures at 4 ½" and 4 ½" x 7" of 19.4 bar and 35.4 bar (see Table 3). The detailed evaluation data including pressure and temperature data is attached in Enclosure 14.

5.3.3 Results at Well 474

The essential test results for well 474 are listed in Table 12. In general, negative leak rates signify an inflow of oil, whereas positive leak rate indicate a loss of oil.

Table 12: 2nd MIT results at well 474

Measurement no.	Time in dd/mm/yy hh:mm	BCS interface level depth in m MD	Calculated oil volume in l	Apparent leak rate of intervals in l/d in-situ
Reference	08/12/2014 13:00	447.5	4,774.5	-
First	09/12/2014 13:00	447.5	4,774.5	0.0
Second	10/12/2014 13:00	447.5	4,774.5	0.0
Third	11/12/2014 13:00	447.5	4,774.5	0.0
Fourth	12/12/2014 13:00	447.5	4,774.5	0.0

During testing time, a constant oil/brine interface level depth of 447.5 m MD was observed from the reference until the fourth measurement (see also Enclosure 11). After brine pumping on 08/12/2014 for pressure readjustment subsequent to the zero measurement, the interface level went up one BCS step to 447.4 m MD. After a damping period overnight, the interface level returned to the depth of 447.5 m MD. This interface movement could be explained by the brine pumping at 4 ½" of well 474. The pumped brine cooled down the oil in the 4 ½" x 7" at well 474. The oil temperature of the BCS reduced from approx. 23 °C to 18 °C. Thus, this interface movement was caused by temperature effects.

Therefore, the apparent leak rates of all intervals were calculated to 0.0 l/d in-situ. This corresponded to an average apparent leak rate for the overall testing time of 0.0 l/d in-situ. The MIT accuracy for well 474 was calculated to +/- 5.1 l/d in-situ, which represented the test criterion (see Table 8). Therewith, the average leak rate stayed within the boundaries of the determined test criterion. The visualisation of the apparent leak rates and of the MIT accuracy is given in Figure 7.

Figure 7: Apparent leak rates of 2nd MIT at well 474

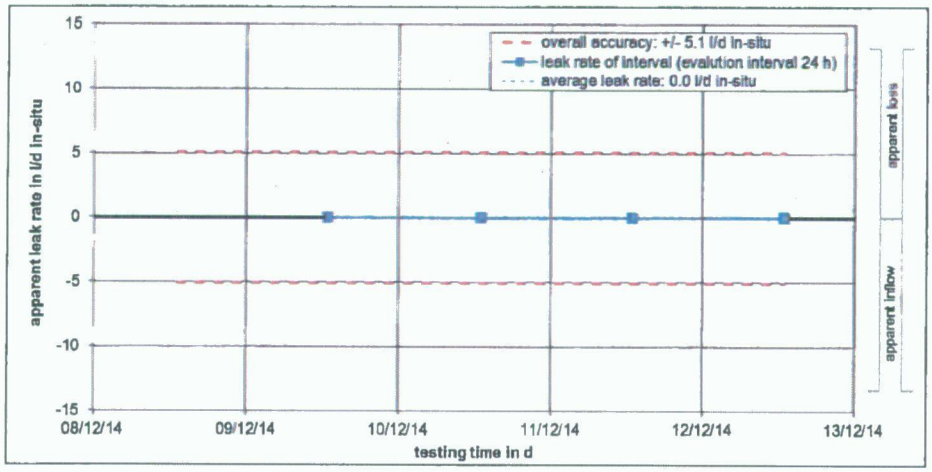

Furthermore, the observed well head pressures during testing time at well 474 were not less than the minimum MIT well head pressures at 4 ½" and 4 ½" x 7" of 19.4 bar and 35.5 bar (see Table 3). The detailed evaluation data including pressure and temperature data is attached in Enclosure 15.

6 Summary and Conclusion

The calculated test accuracies for the MIT at wells 472, 473 and 474 were adequatley exact to allow final statements regarding hydraulic tightness of the LCCS.

All calculated average leak rates of well 472, 473 and 474 stayed within the boundaries of the test accuracies, which determined the test criterion.

Additionally, all observed well head pressures during testing time were not less than the maximum permissible pressures during future oil operation.

Therefore, the last cemented casing shoes of well 472, 473 and 474 of AkzoNobel cavern series 472 can be declared "technically hydraulic tight" with regard to the rock mechanical approved pressures during oil operation.

List of Enclosures

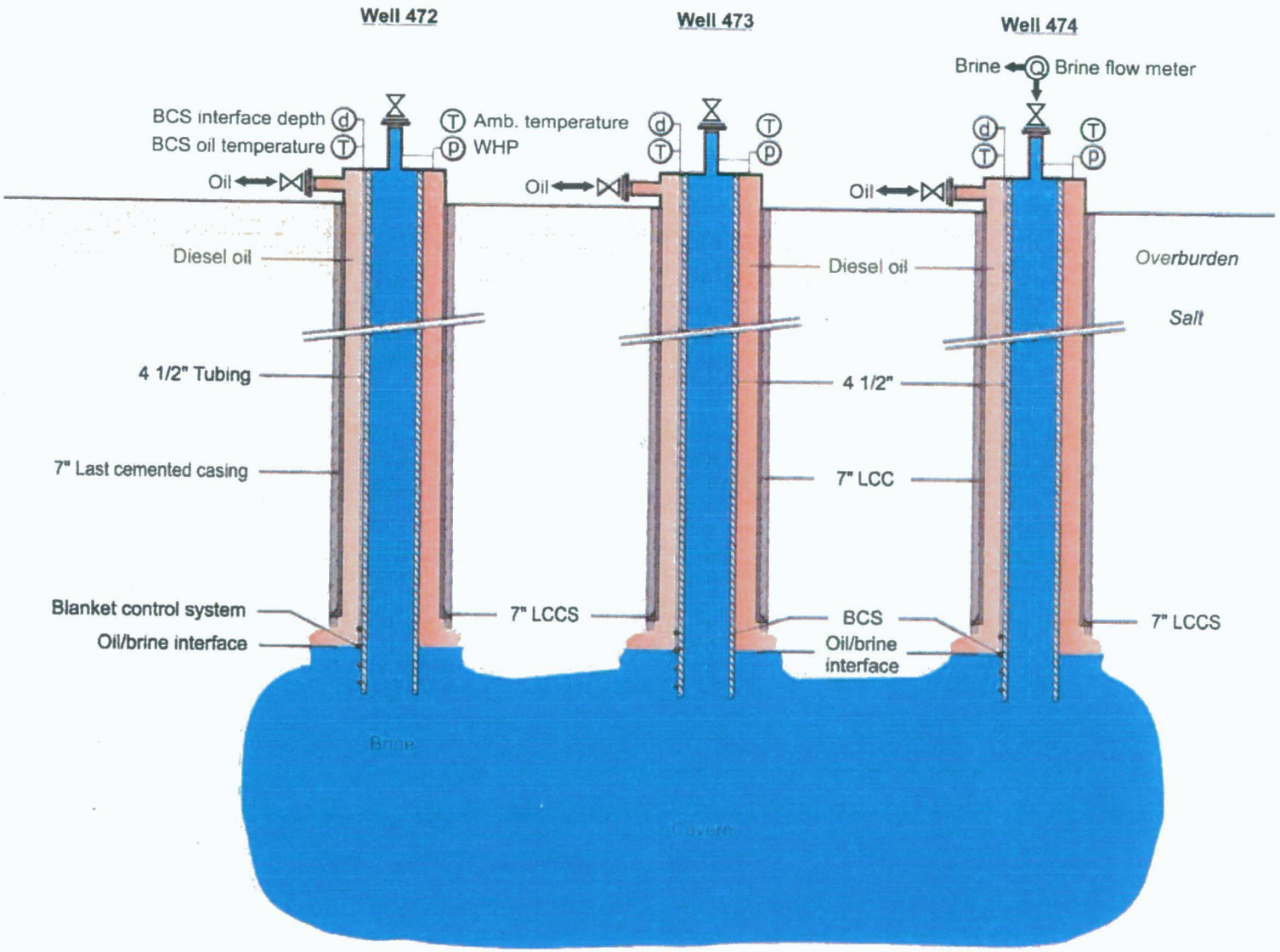

Enclosure 1: 2nd MIT Akzo cavern series 472, MIT setup

141212 2nd MIT Akzo cavern series 472 rev04.xlsx

PN 5305: Cavern neck volume list well 472

7" LCCS at 444.4 m MD
calc. oil volume in 4 1/2" x 7" to 7" LCCS in liter: 4.532.3
calc. oil volume in neck to uppermost BCS sensor in liter: 50.7

level depth in m MD	BCS sensor no.	neck radius in m*	from depth in m MD	to depth in m MD	delta volume 4 1/2" x 7" in liter*	total volume 4 1/2" x 7" in liter
446.6	1	0.144	446.5	446.6	-	4.583.0
446.7	2	0.151	446.6	446.7	6.1	4.589.1
446.8	3	0.152	446.7	446.8	6.3	4.595.4
446.9	4	0.152	446.8	446.9	6.3	4.601.7
447.0	5	0.150	446.9	447.0	6.0	4.607.7
447.1	6	0.153	447.0	447.1	6.3	4.614.0
447.2	7	0.155	447.1	447.2	6.5	4.620.5
447.3	8	0.154	447.2	447.3	6.4	4.626.9
447.4	9	0.155	447.3	447.4	6.5	4.633.4
447.5	10	0.155	447.4	447.5	6.5	4.639.9
447.6	11	0.155	447.5	447.6	6.5	4.646.4
447.7	12	0.154	447.6	447.7	6.4	4.652.8
447.8	13	0.152	447.7	447.8	6.3	4.659.1
447.9	14	0.153	447.8	447.9	6.3	4.665.4
448.0	15	0.153	447.9	448.0	6.4	4.671.8
448.1	16	0.155	448.0	448.1	6.5	4.678.2
448.2	17	0.155	448.1	448.2	6.5	4.684.8
448.3	18	0.152	448.2	448.3	6.2	4.691.0
448.4	19	0.152	448.3	448.4	6.2	4.697.2
448.5	20	0.154	448.4	448.5	6.4	4.703.7

*: based on caliper measurement

Enclosure 2: 2nd MIT Akzo cavern well 472, Cavern neck volume list

PN 5305: Cavern neck volume list well 473

7" LCCS at 443.2 m MD
calc. oil volume in 4 1/2" x 7" to 7" LCCS in liter: 4.520.1
calc. oil volume in neck to uppermost BCS sensor in liter: 1.806.9

level depth in m MD	BCS sensor no.	neck radius in m*	from depth in m MD	to depth in m MD	delta volume 4 1/2" x 7" in liter*	total volume 4 1/2" x 7" in liter
445.2	1	0.226	445.1	445.2	-	6.327.0
445.3	2	0.226	445.2	445.3	15.0	6.341.9
445.4	3	0.223	445.3	445.4	14.6	6.356.5
445.5	4	0.223	445.4	445.5	14.6	6.371.1
445.6	5	0.199	445.5	445.6	11.5	6.382.6
445.7	6	0.199	445.6	445.7	11.5	6.394.0
445.8	7	0.204	445.7	445.8	12.1	6.406.1
445.9	8	0.204	445.8	445.9	12.1	6.418.2
446.0	9	0.205	445.9	446.0	12.2	6.430.4
446.1	10	0.205	446.0	446.1	12.2	6.442.5
446.2	11	0.203	446.1	446.2	11.9	6.454.4
446.3	12	0.203	446.2	446.3	11.9	6.466.3
446.4	13	0.196	446.3	446.4	11.1	6.477.4
446.5	14	0.196	446.4	446.5	11.1	6.488.4
446.6	15	0.182	446.5	446.6	9.4	6.497.8
446.7	16	0.182	446.6	446.7	9.4	6.507.2
446.8	17	0.186	446.7	446.8	9.9	6.517.1
446.9	18	0.186	446.8	446.9	9.9	6.526.9
447.0	19	0.172	446.9	447.0	8.3	6.535.2
447.1	20	0.172	447.0	447.1	8.3	6.543.5

*: based on sonar measurement

Enclosure 3: 2nd MIT Akzo cavern well 473, Cavern neck volume list

141212 2nd MIT Akzo cavern series 472 rev04.xlsx

PN 5305: Cavern neck volume list well 474

7" LCCS at 444.2 m MD
calc. oil volume in 4 1/2" x 7" to 7" LCCS in liter: 4.530.3
calc. oil volume in neck to uppermost BCS sensor in liter: 74.6

level depth in m MD	BCS sensor no.	neck radius in m*	from depth in m MD	to depth in m MD	delta volume 4 1/2" x 7" in liter*	total volume 4 1/2" x 7" in liter
446.4	1	0.188	446.3	446.4	-	4.604.9
446.5	2	0.194	446.4	446.5	10.8	4.615.6
446.6	3	0.217	446.5	446.6	13.8	4.629.4
446.7	4	0.236	446.6	446.7	16.5	4.645.9
446.8	5	0.228	446.7	446.8	15.3	4.661.1
446.9	6	0.228	446.8	446.9	15.4	4.676.5
447.0	7	0.233	446.9	447.0	16.0	4.692.5
447.1	8	0.237	447.0	447.1	16.6	4.709.1
447.2	9	0.233	447.1	447.2	16.0	4.725.1
447.3	10	0.236	447.2	447.3	16.5	4.741.6
447.4	11	0.236	447.3	447.4	16.4	4.758.0
447.5	12	0.237	447.4	447.5	16.6	4.774.5
447.6	13	0.224	447.5	447.6	14.8	4.789.3
447.7	14	0.207	447.6	447.7	12.5	4.801.8
447.8	15	0.221	447.7	447.8	14.3	4.816.1
447.9	16	0.233	447.8	447.9	16.0	4.832.1
448.0	17	0.224	447.9	448.0	14.7	4.846.8
448.1	18	0.195	448.0	448.1	10.9	4.857.7
448.2	19	0.210	448.1	448.2	12.8	4.870.4
448.3	20	0.224	448.2	448.3	14.7	4.885.2

*: based on caliper measurement

Enclosure 4: 2nd MIT Akzo cavern well 474, Cavern neck volume list

141212 2nd MIT Akzo cavern series 472 rev04.xlsx

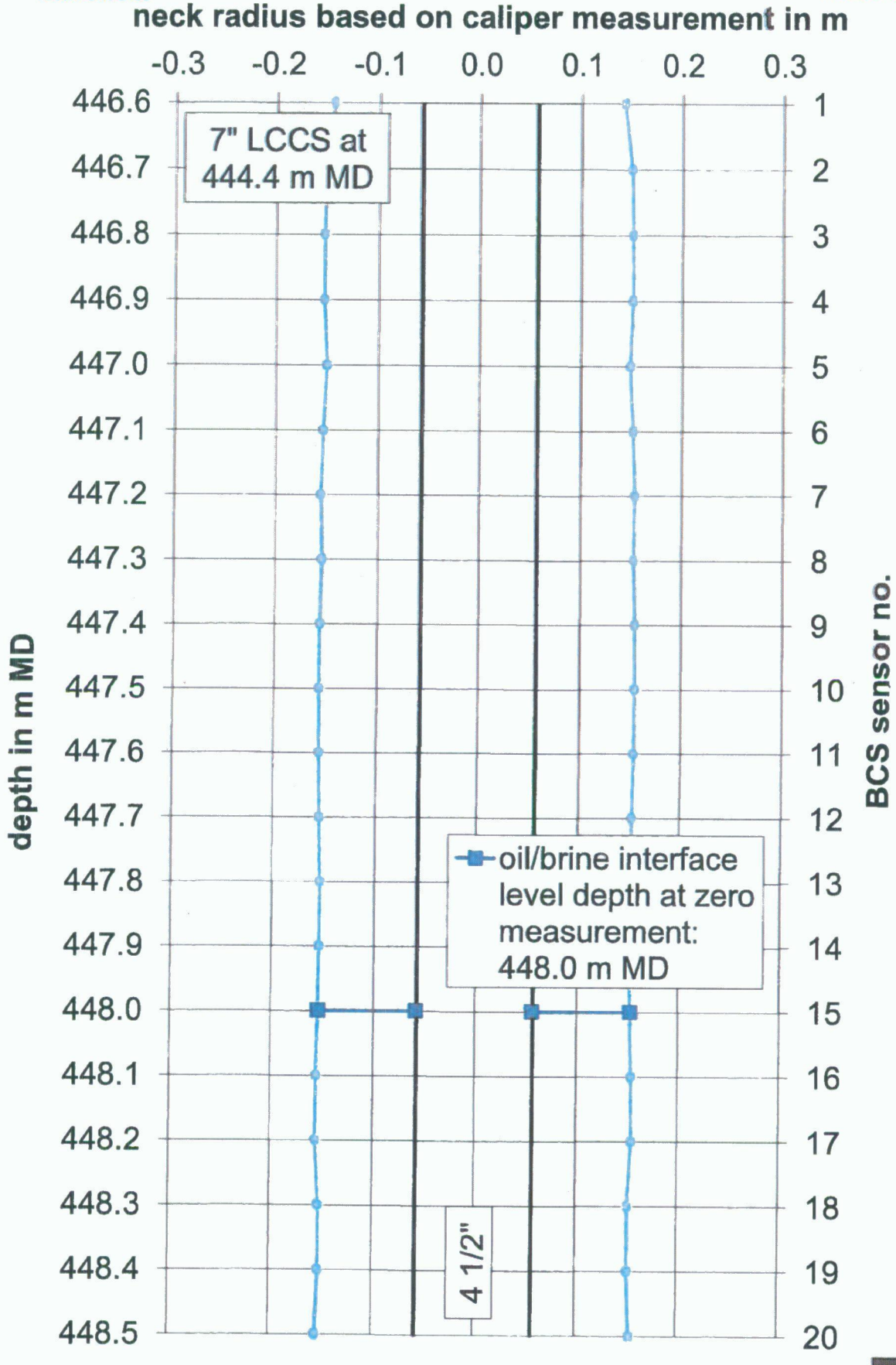

Enclosure 5: 2nd MIT Akzo cavern well 472, Cavern neck